PHOTOACOUSTIC SPECTROSCOPY OF CdS
USING A CW DYE LASER

BY

AWAD HUSEIN ISSA

Supervised by

Dr. I. S. Shahin

" Submitted in Partial Fulfilment of The Requirements for the Degree of Master of Science in Physics, Faculty of Science, University of Jordan."

January 1988

دراسة الطيف الصوتوضوئي لمادة CdS
باستخدام ليزر الأصبغة المستمر

رسالة ماجستير مقدمة من الطالـــــب
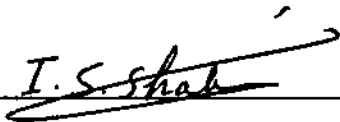عــوض حسيـن عيسـى

باشـراف

الدكتـور عيسـى شاهيـن

" قُدمت هذه الرسالة استكمالا لمتطلبات درجة الماجستير في الفيزياء بكلية العلــوم
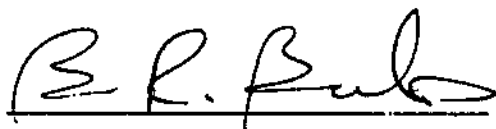في الجامعة الأردنية " .

كانون ثاني، ١٩٨٨ م٠

The Examining Committee unanimously considers this thesis satisfactory for the award of the degree of Master of Science in Physics.

Dr. I. S. Shahin

Chairman of Committee
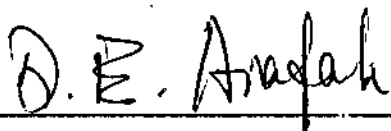Department of Physics
University of Jordan

Dr. B. R. Bulos

Member of Committee
Department of Physics

Dr. M. AL-Haj Abdallah

Member of Committee
Department of Physics

Dr. D. E. Arafah

Member of Committee
Department of Physics

Date: 4/1/1988.

SUMMARY

During the course of this work we succeeded in building a complete experimental setup for Laser Photoacoustic Spectroscopy, including building up necessary mechanical and electronic components at the Department's workshops.

The setup was tested and its performance was evaluated in the light of the Rosenwaig-Gersho (RG) theory of photoacoustic spectroscopy in condensed media.

The photoacoustic spectrum of CdS both as a function of modulating frequency for a fixed wavelength and as a function of wavelength for a fixed frequency were obtained. The log-log curve of the photoacoustic signal with frequency was explained in the light of the RG-theory and the difference in the frequency dependence was explained in terms of the relative values of the thermal diffusion length u and the optical path length l_B. The overlap region between the two frequency domains was determined and a value of $B = 91.3$ cm^{-1} for CdS at $\lambda = 593$ nm was calculated.

Finally the photoacoustic spectrum of CdS with the wavelength was transformed into the corresponding curve for the variation of the optical absorption coefficient B of CdS with the wavelength λ over the whole tunability range of the dye laser.

ملخــــص

لقد تمّ بنجاح خلال هذا البحث بناء نظام تجريبي متكامل للأطياف الصوتوضوئية باستخدام أشعة الليزر ، كما تمّ بناء بعض الأدوات والأجهزة الميكانيكية والألكترونيــــة اللازمة في ورش قسم الفيزياء .

هذا ولقد قمنا بفحص النظام التجريبي عمليا ، مع تقييم أدائه في ضوء نظريـــة روزنتثيك وغيرشو للأطياف الضوتوضوئية في الأجسام الصلبة .

لقد تمّ الحصول على الطيف الصوتوضوئي لمادة CdS كدّالة للتردد عند طــــول موجي معين ، وكدّالة للطول الموجي عند تردد ثابت . هذا وقد أمكن تفسير المنحنـــى اللوغارتمي للطيف الصوتوضوئي مع التردد في ضوء النظرية السابقة كما أمكن تفسير الفرق في اعتماد الطيف على التردد بدلالة القيمة النسبية للطول الانتشاري الحرارى μ_s وطول المسار الضوئي l_β . كما أمكن تحديد منطقة التَّحوُّل بين الترددات المنخفضـــــة والترددات العالية في الطيف الصوتوضوئي المذكورة واستطعنا من ذلك حساب معامــــل الامتصاص الضوئي β حيث كانت قيمته ٢ر٩١ سم$^{-1}$ عند الطول الموجي ٥٩٣ نانومتر .

وأخيرا استطعنا ، باستخدام الطيف الصوتوضوئي مع الطول الموجي، حساب تغيّر معامل الامتصاص الضوئي مع الطول الموجي لمادة CdS على امتداد المدى الموجـي لأشعة ليزر الأصبغة المستخدم .

ACKNOWLEDGEMENTS

I would like to express my gratitude to my supervisor Dr. I. S. Shahin for his help and encouragement during the different stages of this work.

Also I would like to thank the following:

1. The technical staff of the Electronic Workshop who helped in building up some electronic equipment.

2. The technical staff of the Mechanical Workshop who helped in building some mechanical components.

3. Mrs. Mary Shahatit who typed the manuscript.

TABLE OF CONTENTS

Chapter 1

INTRODUCTION

Broadly speaking, spectroscopy can be defined as the study of the interaction of energy with matter. Hence it is a science encompassing many disciplines and many techniques. The energy of interaction in optical spectroscopy is in the form of electromagnetic radiation with wavelengths ranging from less than one Angstrom in the X-ray region to more than 100 microns (10^6 Å) in the far infrared. Because of its versatility, range, and nondestructive nature, optical specroscopy remains one of the most important tools for investigating the properties of matter.

Conventional optical spectroscopies tend to fall into two major categories namely, transmission and reflection spectroscopies respectively. These optical techniques preclude, however, the detection and analysis of radiation absorbed by the material under investigation, even though such a process is often the one most interesting to the investigator. One should also indicate some of the limitations of these conventional spectroscopic methods. For example, conventional transmission spectroscopy is inadequate in measuring very weak absorption which involves the measurement of a very small attenuation of a strong transmitted signal. In addition to weakly absorbing materials there are many substances , both organic and inorganic, that are not readily amenable to the conventional transmission or reflection methods of spectroscopy. These are highly light-scattering

materials, such as powders, amorphous solids, gels, smears, and suspensions. Other difficult materials are those that are optically opaque and have dimensions that far exceed the penetration depth of the optical radiation.

Over the years, several techniques have been developed to permit optical studies of highly light-scattering and opaque substances. The most common of these are diffuse reflectance[1], attenuated total reflection[2], internal reflection spectroscopy[3], and Raman scattering[4]. All these methods have proven to be useful, yet each suffers from serious limitations. In particular, each method is applicable to a relatively small group of materials over a small wavelength range, and the data obtained are often difficult to interpret.

During the last two decades, an old optical technique has been redeveloped to study those materials which are not suitable for the conventional transmission or reflection techniques. This old new method is called photoacoustic spectroscopy PAS[5] and it differs from the conventional techniques in that the interaction of the incident electromagnetic radiation is studied through a direct measure of the energy absorbed by the investigated material as a result of its interaction with the photon beam. It should, however, be kept in mind that a photoacoustic signal could be generated through the absorption of particle energy resulting from electron or ion beam bombardment.

Although the experimental methodology of PAS will be discussed later in chapter 3, yet a brief description seems appropriate at this stage (Fig 1.1). The sample, solid liquid or gas, is often placed in a closed cell containing also a sensitive microphone. The sample is illuminated with monochromatic light which is intensity modulated by an electromechanical chopper or some other method. When some of the incident energy is absorbed by the sample, internal energy levels within the sample are excited. Upon subsequent deexcitation of these levels all or part of the absorbed photon energy is transformed into heat through nonradiative deexcitation processes. In a gas sample heat energy appears as kinetic energy of the gas molecules, while in a solid or liquid, it appears as vibrational energy of ions or atoms. Now since the incident radiation is intensity modulated, the internal heating of the sample will also be modulated.

Since in PAS we measure the internal heating of the sample, it is clearly a form of calorimetry, as well as a form of optical spectroscopy. However conventional calorimetric detection methods based on the use of a calorimeter and the usual temperature sensors such as thermistors and thermopiles, though simple and well developed, have several inherent disadvantages for photoacoustic spectroscopy in terms of sensitivity, detector rise time, and the speed at which measurements can be made. More suitable calorimetric techniques measure heat production
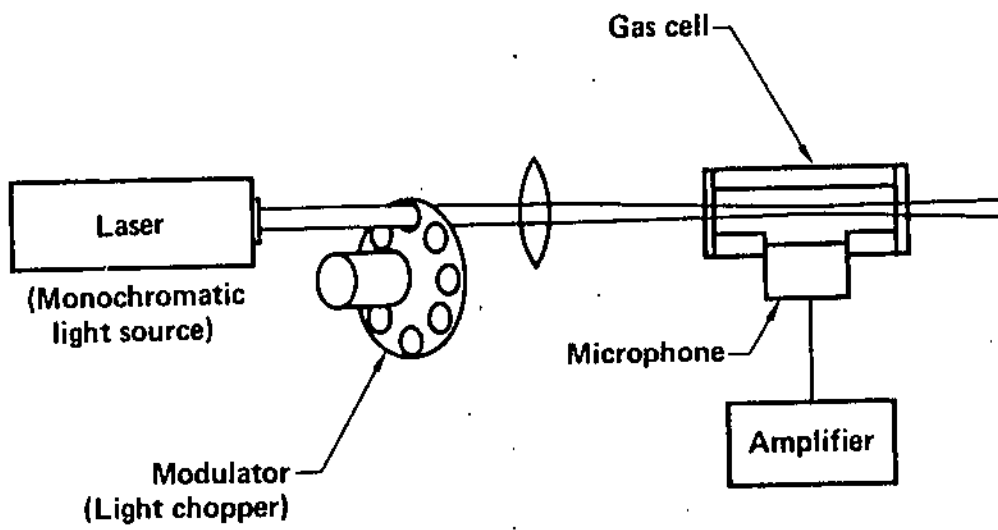
Figure 1.1 Block diagram of a modern gas photoacoustic spectrometer.

through volume and pressure changes produced in the sample (and picked up by a sensitive microphone) or in an appropriate transducing material (such as a piezoelectric detector) in contact with the sample.

Present microphones and associated electronics can detect temperature rises in a gas of 10^{-6} ^{o}C, corresponding to a thermal input of about 10^{-9} calories/cm^{3}. sec. The primary disadvantage of the microphone calorimetric detection method is that the response time is limited both by the transit time for a sound wave in the gas within the cell cavity and by the relatively low-frequency response of the microphone. These two factors together tend to limit the response time of a gas microphone system to about 100μs or longer.

In liquids, or bulk solid samples heat production can be measured through subsequent pressure or stress variations in the sample itself by a piezoelectric detector in intimate contact with the sample. These transducers can detect temperature changes of 10^{-7} to 10^{-6} ^{o}C corresponding, for typical solids and liquids, to thermal inputs of about 10^{-6} calories/cm^{3}. sec. It should be borne in mind, however, that since the coefficient of volume expansion of liquids and solids is 10-100 times smaller than that of gases, measurement of heat production in liquids and solids directly with a microphone would be 10-100 times less sensitive than using a piezoelectric transducer in direct contant with the sample.

When a piezoelectric detector cannot be used, as in the case of a powdered sample, or a smear or gel, a gas (air) is used as a transducing medium coupling the sample to a microphone. The periodic heating of the sample from the absorption of the modulated incident radiation results in a periodic heat flow from the sample to the gas, which itself does not absorb the incident radiation. This in turn produces pressure and volume changes in the gas that drives the microphone. This method is quite sensitive for solids with large surface to volume ratios such as powders, and is capable of detecting temperature rises of 10^{-6} to 10^{-5} ^{o}C corresponding to thermal input of about 10^{-5} to 10^{-6} calories/cm^3. sec.

There are several advantages to photoacoustic spectroscopy. Since <u>absorption</u> of incident radiation is required for the generation of a photoacoustic signal, light which is transmitted or elastically scattered by the sample is not detected and thus does not interfere with the PAS signal. This is of crucial importance for essentially weakly absorbing transparent media, or highly light-scattering materials, such as powders, amorphous solids, gels, and colloids. Another advantage is the capability of obtaining optical absorption spectra of completely opaque materials since the technique does not depend on the detection of photons. Also, unique to photoacoustic spectroscopy is the capability of performing nondestructive depth-profile analysis of absorption as a function of depth inside the material.

Since the sample in PAS plays the role of the electro-magnetic radiation detector, no photoelectric device is necessary, and hence studies over a wide range of the incident radiation are possible without changing the detection system. The only limitations are that the source be sufficiently energetic (at least $10\mu W/cm^2$) and that the windows used be reasonably transparent to the incident radiation. Finally since the PAS signals arise, from a radiationless conversion process, it is complementary to radiative and photochemical processes. Thus PAS may be used as a sensitive indirect method for studying the phenomena of fluorescence and photosensitivity in matter.

It should be pointed out however that PAS is much more than a spectroscopic technique. As a spectroscopic tool it can be used to measure the absorption or excitation spectrum[6], the lifetime of excited states of matter[7], and the energy yield of radiative processes[8]. On the other hand PAS can be used to measure thermal and elastic properties of materials[9], to study chemical reactions[10], to measure thicknesses of layers and thin films[11] and many other nonspectroscopic investigations. In such studies the calorimetric or acoustic aspect of PAS plays the dominant role, while the electromagnetic radiation is simply a convenient excitation mechanism.

With the previous wide scope properties of PAS, the technique has found many important applications in pure and applied

research. The technique is applicable to all types of materials, inorganic, organic and biological, and on all phases of matter—gas, liquid, and solid.

The purpose of the present research is to build and test a reliable experimental setup for photoacoustic spectroscopy and to use it for spectroscopic studies in cadmium sulphide (CdS) powder. Before describing the experimental setup and the results obtained using it, we have to review the basic theory of PAS in solid media. The results of such a theory are crucial for the analysis and understanding of our experimental data.

350695

Chapter 2

General Theory of The Photoacoustic

Effect in Condensed Media:

The Gas Coupling Method

Chapter Two

General Theory Of The Photoacoustic Effect In
Condensed Media: The Gas-Coupling Method

2.1 Introduction

The modern theory of photoacoustics in condensed media is
still not complete, although considerable progress has been
made in the last two decades. The use of a gas-phase micro-
phone and obtaining photoacoustic spectra of solids and liquids
began with the work of Hey and Gollnick[6], Harshbarger and Robins[7],
and Rosencwaig[8]. The PA signal was generated by sinusoidally
modulated cw light beam incident on the condensed sample, and
the periodic heating of the gas at the irradiated surface of
the sample generated the acoustic wave, which was detected by
a gas-phase microphone. The first attempt at a modern, quan-
titative theory was made in 1973 by Parker[9] who derived the
theoretical expression of the PA signal that would be
observed from weak absorptions in esentially transparent
windows. However many of the prominent features of the more
general photoacoustic spectroscopic (PAS) theories can be
found in Parker's previous special treatment.

A more general theory for the photoacoustic effect in
condensed media was formulated, some years later, by Rosencwaig
and Gersho[10] . This theory, now commonly referrd to as the RG
theory, or " gas-piston " model, shows that the PAS signal

depends on the generation of an acoustic pressure disturbance
at the sample-gas interface and on the transport of this dis-
turbance through the coupling gas to the microphone. This
sample-gas disturbance depends in turn on the periodic tempera-
ture at the interface. The RG theory derived exact expre-
ssions for this temperature, while it treated the transport of
the disturbance in the gas in an approximate heuristic manner
which is, however, valid for most experimental conditions.

The general theory was later refined by Bennet and
Forman[11], Aamodt et al[12], and Wetsel and McDonald[13] who treated
the transport of the acoustic disturbance in the gas more
exactly using Navier-Stakes equations. These refinements were
able to account for observed deviations from the RG theory
at very low frequencies and at frequencies near the cell
resonances. There has been a further refinement to the theory
by McDonald and Wetsel[14], who have included contributions to
the signal from thermally induced vibrations in the sample.
Figure 2.1 shows a block diagram explaining the method of
photoacoustic detection in condensed media using gas coupling
as will be discussed in the next section.

In this chapter we shall review the RG general theory
and consider some of the later improvements. The basic results
of the theory will be used to interpret our experimental data
on cadmium sulphide CdS.

Front Window

Condensed Sample

Coupling Gas

Backing Material

ℓ

ℓ'

Periodic Optical Absorption

Light Modulated at Frequency f

B

Heat Generated in Absorption Length

Acoustic Waves in Sample, Causing Interface to Oscillate

Sound Propagation in Gas

Heat Within Thermal Diffusion Length Communicates with Interface

Thin Layer of Gas Heated Periodically

Sound Generation and Propagation in the Gas

Detection by Microphone
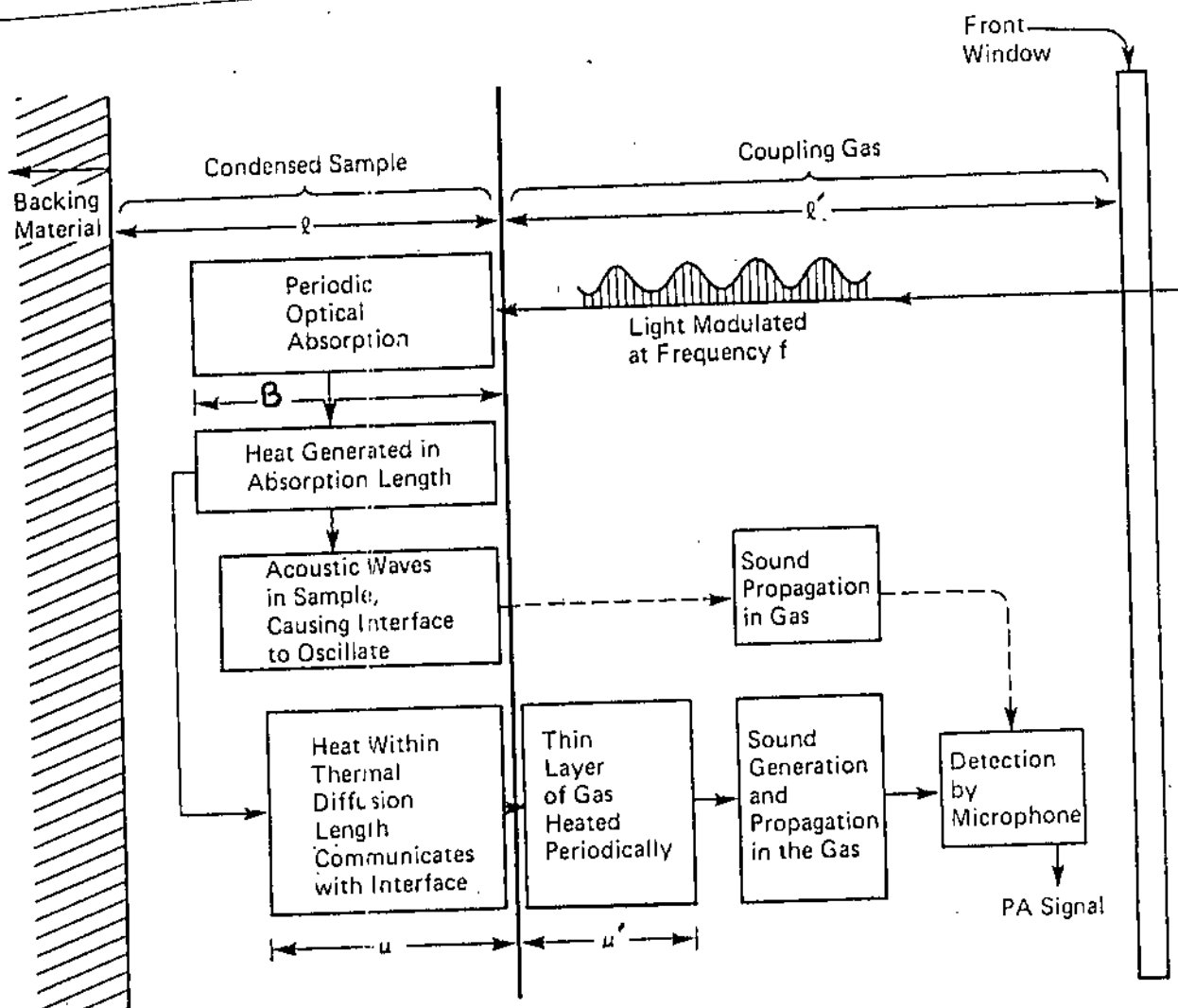
PA Signal

μ

μ'

Fig. 2.1 Block diagram to explain the method of PA detection in condensed matter using gas coupling.

2.2   The Rosencwaig-Gersho Theory

2.2.1   The Thermal Diffusion Equations

We shall carry out a one-dimensional analysis for the production of a PA signal in a simple cylindrical cell as shown in Fig. 2.2.   The cell has a diameter D, and length L which is small compared to the wavelength of the acoustic signal.   The sample in disc form of diameter D and length l is resting tightly against a poor thermal conductor backing of thickness l''. The length l' of the gas column in the cell is given by l' = L-l-l".   We further assume that the gas and backing materials do not absorb light.

We now define the following parameters

k : the thermal conductivity (cal/cm.s.^{o}C),

ρ : the density (g/cm^3)

C : the specific heat (cal/g.^{o}C),

α = k/ρC: the thermal diffusivity (cm^2/s),

a = (w/2α)$^{\frac{1}{2}}$: the thermal diffusion coefficient (cm^{-1}),

u = $\dfrac{1}{a}$: the thermal diffusion length (cm).

where w is the chopping frequency of the incident light in radian per second (rad/s).   In the following treatment, we denote sample parameters by unprimed symbols, gas parameters by single primed symbols, and backing material by doubly primed symbols.

The basic idea of the theory of PA generation is represented in Fig. 2.1. The periodic heating of the sample occurs in the optical "absorption length" defined by,

$$1_B = \frac{1}{B} \qquad (2.1)$$

where B is the absorption coefficient (cm^{-1}) of the incident optical beam in the sample. However, only the heat within a diffusion length μ from the interface can communicate with the coupling gas and heat up a gas layer of length u' which expands periodically, producing acoustic waves. This is the essence of the RG theory or "gas-piston" model.

McDonald and Wetsel[14] suggested that in some cases, additional effects may be generated owing to the acoustic wave produced in the sample causing the interface itself to vibrate as indicated in Fig. 2.1. This effect is frequently small compared to that of the gas piston. This is, however, not the case when the sample is sufficiently transparent ($B < 1$ cm^{-1}) and the modulation frequency f is sufficiently large ($f > 10^3$ Hz). When this happens a "composite piston" model must be used because the gas-piston effect and the sample surface vibration effect may both contribute significantly to the observed PA signal.

Now let a sinusoidally chopped monochromatic light beam of wavelength λ be incident on the sample with intensity,

$$I = \frac{1}{2} I_o (1 + \cos wt) \qquad (2.2)$$

where I_o is the premodulation intensity of the beam (W/cm^2). The heat density (W/cm^3) produced at any point x due to light absorbed at this point inside the sample is then

$$\frac{1}{2} B I_o e^{Bx} (1 + \cos wt) \qquad (2.3)$$

where x takes on negative values since the sample extends from $x = o$ to $x = -l$, with the light incident at $x = o$ (Fig. 2.2). Note also that the air column extends from $x = o$ to $x = l'$, and the backing from $x = -l$ to $x = -(l + l'')$.

The thermal diffusion equation in the sample taking the distributed heat source into consideration is

$$\frac{\partial^2 \theta}{\partial x^2} = \frac{1}{\alpha} \frac{\partial \theta}{\partial t} - Ae^{Bx}(1+e^{iwt}) \quad \text{for } -l \leq x \leq o \qquad (2.4)$$

with

$$A = \frac{B I_o \eta}{2k} \qquad (2.5)$$

where θ is the temperature and η is the efficiency at which the modulated absorbed light at wavelength λ is converted to heat by the nonradiative deexcitation processes. For most solids $\eta = 1$ at room temperature. The corresponding heat diffusion equations for the backing and the gas are respectively

$$\frac{\partial^2 \theta}{\partial x^2} = \frac{1}{\alpha''} \frac{\partial \theta}{\partial t} \qquad -l''-l \leq x \leq -l \qquad (2.6)$$
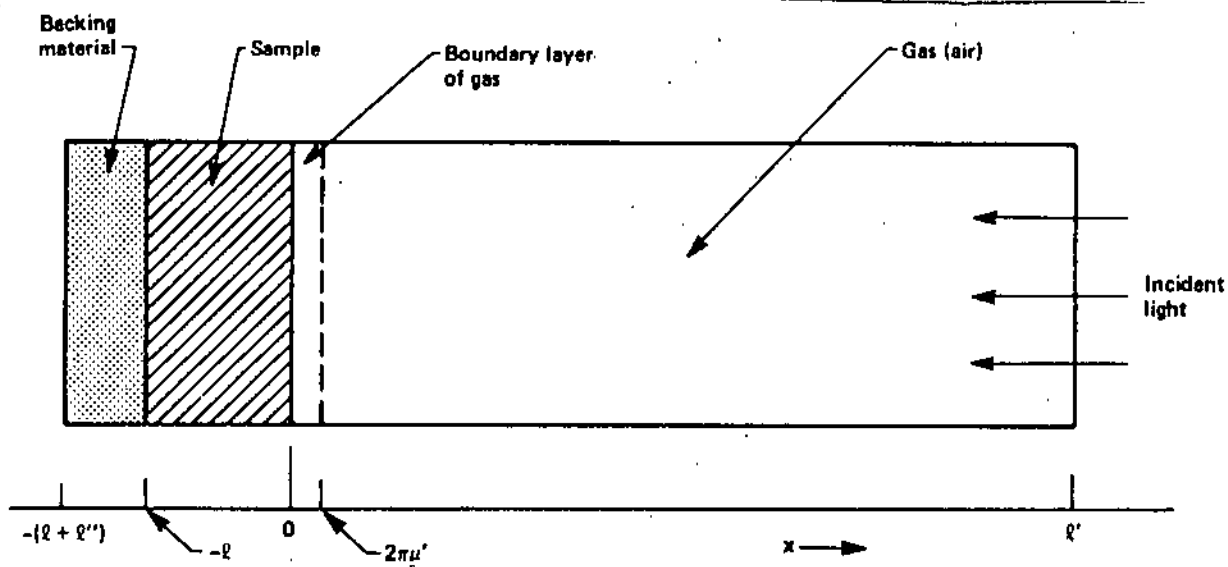
Figure 2.2 Cross-sectional view of a simple cylindrical photoacoustic cell.

$$\frac{\partial^2 \theta}{\partial x^2} = \frac{1}{\alpha'} \frac{\partial \theta}{\partial t} \qquad 0 \leq x \leq 1' \qquad (2.7)$$

The real part of the complex valued solution $\theta(x,t)$ of the equations (2.3) to (2.6) represents the temperature in the cell relative to ambient temperature ϕ_0. Thus the actual temperature field in the cell is given by

$$T(x,t) = \text{Re } \theta(x,t) + \phi_0 \qquad (2.8)$$

The appropriate boundary conditions are obtained from the requirement of temperature and heat flux continuity at the boundaries $x = 0$ and $x = -1$, and from the constraint that the temperature at the cell walls $x = +1'$ and $x = -1-1''$ is at the ambient (room) temperature. Finally we assume that the cell dimensions are small enough to ignore convective heat flow in the gas under steady-state conditions.

2.2.2 Temperature Distribution in the Cell

The general solution $\theta(x,t)$ in the cell neglecting transients can be written as

$$\theta(x,t) = \begin{cases} \frac{1}{1''}(x+1+1'') \ W_0 + W e^{\sigma''(x+1)} e^{i w t} & -1-1'' \leq x \leq -1 \\ b_1 + b_2 + b_3 e^{\beta x} + (U e^{\sigma x} + V e^{-\sigma x} - E e^{\beta x}) e^{i w t} & -1 \leq x \leq 0 \\ (1-\frac{x}{1'}) F + \theta_0 e^{-\sigma' x} e^{i w t} & 0 \leq x \leq 1' \end{cases} \qquad (2.9)$$

where $W, U, V, E,$ and θ_0 are complex valued constants; b_1, b_2, b_3, W_0, and F are real valued constants, and $\delta = (1+i)a$ with $a = (w/2\alpha)^{\frac{1}{2}}$. In fact θ_0 and W represent the complex amplitudes of the periodic temperatures at the sample-gas boundary $(x = o)$ and the sample-backing boundary $(x = -1)$, respectively. The d.c solution in the backing and gas already make use of the boundary condition that the temperature, relative to ambient, is zero at the ends of the cell $x = -1-1''$ and $x = 1'$. W_0 and F denote the d.c component of temperature, relative to ambient, at the sample surface $x = -1$ and $x = o$, respectively. The quantities E and b_3, determined by the forcing function in eq. 2.3, are given by

$$b_3 = \frac{-A}{B^2} \qquad\qquad (2.10)$$

$$E = \frac{A}{(B^2 - \delta^2)} = \frac{\beta I_0}{2k(B^2 - \delta^2)} \qquad\qquad (2.11)$$

In the general solution 2.9 we omit the growing exponential component of the solutions to the gas and backing material because $u'' < 1$ and $u' < 1'$ for all frequencies w of interest ($u' \sim 0.02$ cm for air when $w = 630$ rad/s). Hence the sinusoidal components of these growing solutions are sufficiently damped and are effectively zero at the cell walls. Therefore, to satisfy the temperature constraint at the cell walls, the growing exponential components of the solutions would have essentially zero coefficients.

The temperature and flux continuity conditons at the
sample surfaces $x = o$, and $x = -1$ are given by

$$\theta'(o,t) = \theta(o,t) \tag{2.12a}$$

$$\theta''(-1,t) = \theta(-1,t) \tag{2.12b}$$

$$k' \frac{\partial \theta'}{\partial x}(o,t) = k \frac{\partial \theta}{\partial x}(o,t) \tag{2.12c}$$

$$k'' \frac{\partial \theta''}{\partial x}(-1,t) = k \frac{\partial \theta}{\partial x}(-1,t) \tag{1.12d}$$

These boundary conditions apply separately to the d.c component
and a.c component of the solution. Applying (2.12) to the d.c
component of the solution 2.9 gives

$$F_o = b_1 + b_3 \tag{2.13a}$$

$$W_o = b_1 - b_2 l + b_3 e^{-Bl} \tag{2.13b}$$

$$\frac{-k'}{l'} F_o = kb_2 + kBb_3 \tag{2.13c}$$

$$\frac{k''}{l''} W_o = kb_2 + kBb_3 e^{-Bl} \tag{2.13d}$$

Equations 2.13 determine the coefficients b_1, b_2, b_3, W_o and
F_o for the time-independent (d.c) component of the solution.
Again applying the constraints (2.12) to the a.c component of
the solution 2.9 gives

$$\theta_0 = U + V - E \qquad (2.14a)$$

$$W = e^{-\delta l} U + e^{\delta l} V - e^{-\beta l} E \qquad (2.14b)$$

$$-k'\delta'\theta_0 = k\delta U - k\delta V - k\beta E \qquad (2.14c)$$

$$k''\delta''W = k\delta e^{-\delta l} U - k\delta e^{\delta l} V - k\beta e^{-\beta l} E \qquad (2.14d)$$

These equations together with 2.11 determine the coefficients U,V,W, and θ_0. With the determination of all arbitrary constants using equations 2.13 and 2.14, we can determine the temperature distribution (2.8) in the cell in terms of the optical, thermal, and geometric parameters of the system. The explicit expression of θ_0, the complex amplitude of the periodic temperature at the solid-gas (x = o) boundary is given by

$$\theta_0 = \frac{\beta I_0}{2K(\beta^2 - \delta^2)} \cdot \frac{(r-1)(b+1)e^{\delta l} - (r+1)(b-1)e^{-\delta l} + 2(b-r)e^{-\beta l}}{(g+1)(b+1)e^{\delta l} - (g-1)(b-1)e^{-\delta l}} \qquad (2.15)$$

where

$$b = \frac{k''a''}{ka} \qquad (2.16)$$

$$g = \frac{k'a'}{ka} \qquad (2.17)$$

$$r = (1-i)\frac{\beta}{2a} \qquad (2.18)$$

and $\delta = (1+i)a$, as stated before. Eq. 2.15 can be evaluated

for specific parameter values, yielding a complex number whose real and imaginary parts, θ_1 and θ_2 respectively determine the in-phase and quadrature components of the periodic temperature variation at x = o for the sample. Specifically, the actual temperature at x = o is given by

$$T(0, t) = \phi_0 + F_0 + \theta_1 \cos wt - \theta_2 \sin wt \qquad (2.19)$$

where ϕ_0 is the ambient temperature at the cell walls and F_0 is the increase in temperature due to the steady-state (d.c) component of the absorbed heat.

2.2.3 Production of The Acoustic Signal

As previously indicated, the acoustic signal arizes from the periodic heat flow from the solid to the surrounding gas. The periodic diffusion process produces a periodic temperature variation in the gas as given by the a.c component of the sol- ulation 2.9 for $o \leqslant x \leqslant \mathscr{l}$, that is

$$\theta_{a.c.}(x,t) = \theta_0 \, e^{-\delta' x} e^{iwt} \qquad (2.20)$$

With $\delta' = (1+i)a'$ we see, by taking the real part of 2.20, that the actual physical temperature variation in the gas is

$$T_{a.c.}(x,t) = e^{-a'x} \left[\theta_1 \cos(wt-a'x)-\theta_2 \sin(wt-a'x) \right] \quad (2.21)$$

where θ_1 and θ_2 are the real and imaginary parts of θ_2, as given by (2-15). It is obvious from eq. 2.21 that $T_{a.c}(x,t)$

is fully damped out at a distance $x = \frac{2\pi}{a'} = 2\pi u'$ from the solid-gas boundary, where u' is the thermal diffusion length in the gas. Thus we can define a boundary layer (see Fig. 2.1), whose thickness is $2\pi u'$ (0.1 cm at $\frac{w}{2\pi}$ = 100 Hz) and assume, to a good approximation, that only this layer of gas responds thermally to the periodic temperature at the surface of the sample.

The spatially averaged temperature of the gas within the previous boundary layer is given by

$$\bar{\theta}(t) = \frac{1}{2\pi u'} \int_0^{2\pi u'} \theta_{a.c.}(x,t)\, dx \qquad (2.22)$$

Substituting for $\theta_{a.c}$ from eq. 2.20 and using the approximation $e^{-2\pi} \ll 1$ we get

$$\bar{\theta}(t) \simeq \frac{1}{2\sqrt{2}\,\pi} \theta_0\, e^{i(wt - \pi/4)} \qquad (2.23)$$

This layer of gas acts as an acoustic piston on the rest of the gas column, producing a periodic acoustic pressure signal that travels through the entire gas column. The displacement x(t) of this gas piston due to the periodic heating can be estimated using the ideal gas law

$$\frac{\delta x(t)}{\bar{\theta}(t)} \qquad \frac{2\pi u'}{T_0}$$

or, substituting for $\theta(t)$ from eq. 2.23 we get

$$\delta x(t) = \frac{\theta_0 \, u'}{\sqrt{2} \, T_0} \, e^{i(wt - \pi/4)} \qquad (2.24)$$

where we have set the average d.c. temperature of the boundary gas layer equal to the d.c. temperature at the solid surface, that is $T_0 = \phi_0 + f_0$. This is a reasonable approximation in view of the fact $2\pi u'$ is only ~ 0.1 cm at a frequency of 100 Hz and gets even smaller at higher frequencies.

If we now assume that the rest of the gas responds to the action of this piston adiabatically, then the acoustic pressure in the cell due to the displacement $\delta x(t)$ of this piston is derived from the adiabatic gas law

$$PV^{\gamma} = \text{constant} \qquad (2.25)$$

If P_0 and V_0 are the ambient pressure and volume respectively inside the gas cell, then the incremental pressure is given by

$$\delta P(t) = \frac{\gamma P_0 \delta V}{V_0} = \frac{\gamma P_0}{l} \, \delta x(t) \qquad (2.26)$$

where we have used the fact that $\delta V/V_0 = \delta x(t)/l'$.
Now substituting for $\delta x(t)$ from eq. 2.24 we get

$$\delta P(t) = \frac{\gamma P_o \theta_o}{\sqrt{2} \; l'a'T_o} \; e^{i(wt - \pi/4)} \qquad (2.27)$$

or

$$\delta P(t) = Q \; e^{i(wt - \pi/4)} \qquad (2.28)$$

where

$$Q = \frac{\gamma P_o \theta_o}{\sqrt{2} \; l'a'T_o} \qquad (2.29)$$

Bearing in mind that θ_o (eq. 2.15 is complex we can put

$$Q = Q_1 + iQ_2 = ge^{-i\psi} \qquad (2.30)$$

Now using eq. 2.30 in eq. 2.28 and taking the real part $\Delta p(t)$ of $\delta P(t)$ as the actual physical pressure variation we get

$$\Delta p(t) = Q_1 \cos(wt - \frac{\pi}{4}) - Q_2 \sin(wt - \frac{\pi}{4}) \qquad (2.31)$$

or

$$\Delta p(t) = q \cos(wt - \psi - \frac{\pi}{4}) \qquad (2.32)$$

In fact Q specifies the complex envelope of the sinusoidal pressure variation. The explicit formula for Q is obtained by substituting for θ_o from eq. 2.15 in eq. 2.29 where we get

$$Q = \frac{BI_o \gamma P_o}{2\sqrt{2} \; T_o kl'a'(B^2 - \delta^2)} \frac{(r-1)(b+1)e^{\delta 1} - (r+1)(b-1)e^{-\delta 1} + 2(b-r)e^{-B1}}{(g+1)(b+1)\; e^{\delta 1} - (g-1)(b-1)e^{-\delta 1}} \qquad (2.33)$$

where $b = k'' a''/ka$, $g = k'a'/ka$, $r = (1-i)B/2a$, and $\beta = (1+i)a$ as defined earlier. At ordinary temperatures $T_0 \simeq \theta_0$ so that the d.c. components of the temperature need not be evaluated. Thus using eq. 2.33 we can evaluate the magnitude and phase of the acoustic pressure wave produced in the cell by the photo-acoustic effect.

2.3 Special Cases.

It is relatively difficult to explain the full expression for $\Delta p(t)$ of eq. 2.32 because of the complicated expression of Q as given by eq. 2.33. However, we gain physical insight by examining special cases where eq. 2.33 becomes relatively simple. These special cases are grouped into two main categories namely, (1) optically transparent solids with $l_\beta \gg l$; and (2) optically opaque solids with $l_\beta \ll l$, where

$$ l_B = \frac{1}{B} \qquad (2.34) $$

is the optical absorption length, and l is the thickness of the solid. Now for each main category of optical opaqueness we consider three cases according to the relative magnitude of the thermal diffusion length u as compared to l and l_B. For all the cases evaluated below, we make use of the reasonable assumption that $g < b$ and $b \sim 1$ which means that $k'a' < k''a''$ and $k''a'' \simeq ka$. The previous six cases are shown in Fig. 2.2 where we have defined
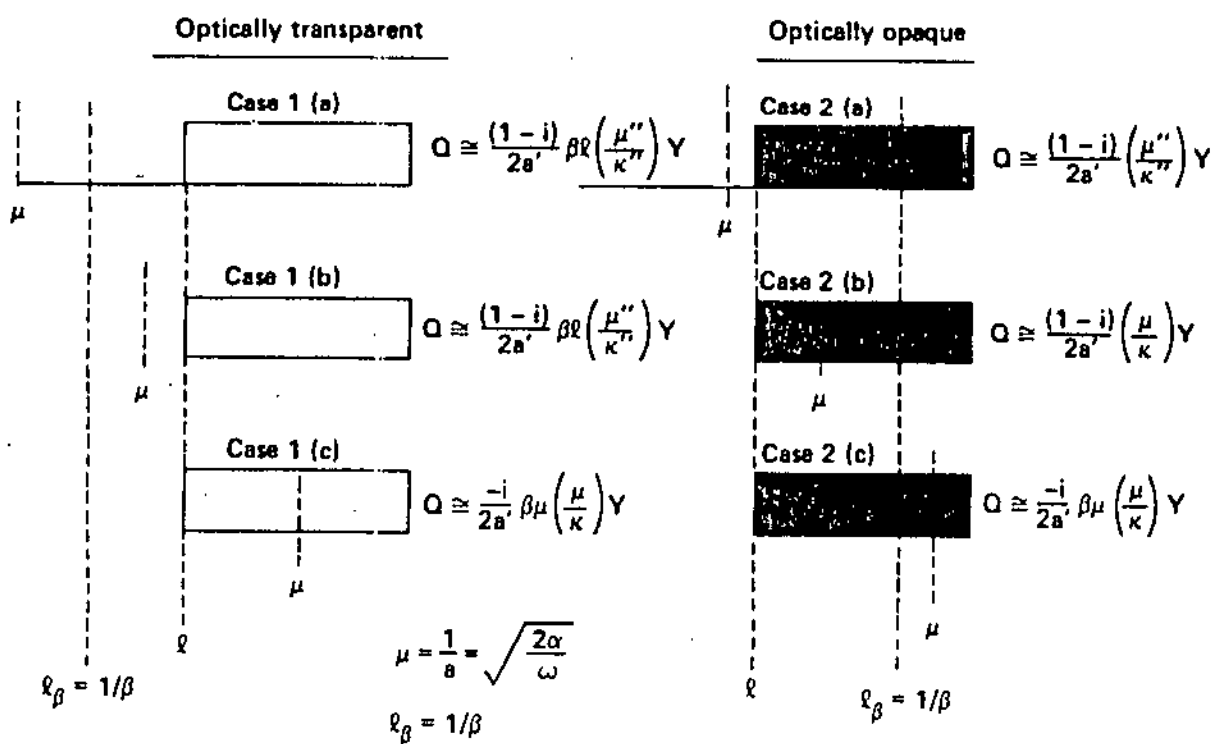
Optically transparent

Optically opaque

Case 1 (a)

$Q \cong \frac{(1-i)}{2a'} \beta\ell\left(\frac{\mu''}{\kappa''}\right)Y$

Case 2 (a)

$Q \cong \frac{(1-i)}{2a'}\left(\frac{\mu''}{\kappa''}\right)Y$

μ

μ

Case 1 (b)

$Q \cong \frac{(1-i)}{2a'} \beta\ell\left(\frac{\mu''}{\kappa''}\right)Y$

Case 2 (b)

$Q \cong \frac{(1-i)}{2a'}\left(\frac{\mu}{\kappa}\right)Y$

μ

μ

Case 1 (c)

$Q \cong \frac{-i}{2a'} \beta\mu\left(\frac{\mu}{\kappa}\right)Y$

Case 2 (c)

$Q \cong \frac{-i}{2a'} \beta\mu\left(\frac{\mu}{\kappa}\right)Y$

μ

μ

ℓ

ℓ

$\mu = \frac{1}{a} = \sqrt{\frac{2\alpha}{\omega}}$

$\ell_\beta = 1/\beta$

$\ell_\beta = 1/\beta$

$\ell_\beta = 1/\beta$

Figure 2.3 Schematic representation of the special cases for the photoacoustic theory of solids.

$$Y = \frac{VP_o\, I_o}{2\sqrt{2}\ T_o\ l'} \tag{2.35}$$

2.3.1 Optically Transparent Solids ($l_\beta > l$)

In these cases, the light is absorbed throughout the length of the sample, and some light is transmitted through the sample.

Case 1a: Thermally thin Solids ($u \gg l$; $u > l_\beta$). here we put $e^{-\beta l} \simeq 1 - \beta l$, $e^{\pm \sigma l} \simeq 1$, and $|r| > 1$ in eq. 2.33. We then obtain

$$Q = \frac{Y}{2a'a''k''}\ (\beta - 2ab - i\beta) \simeq \frac{(1-i)\beta l}{2a'}\ \left(\frac{u''}{k''}\right)\ Y \tag{2.36}$$

In this case the acoustic signal is proportional to β ; since u''/a' is proportional to $1/w$, the acoustic signal has an $\bar{w}^{-1}$ dependence. Moreover the thermal properties of the backing material affect Q through the parameter (u''/k'').

Case 1b: Thermally Thin Solids ($u > l$; $u < l_\beta$) Here we put $e^{-\beta l} \simeq 1 - \beta$, $e^{\pm \sigma l} \simeq (1 \pm \sigma l)$, and $|r| < 1$ in eq. 2.33. We then get

$$Q = \frac{\beta l Y}{4ka'a^3 b}\left[(\beta^2 + 2a^2) + i(\beta^2 - 2a^2)\right] \simeq \frac{(1-i)\beta l}{2a'}\ \left(\frac{u''}{k''}\right) Y \tag{2.37}$$

Eq. 2.37 is identical to eq. 2.36 with identical consequences.

Case 1c: Thermally Thick Solids ($u < 1$; $u \ll 1_B$)

Here we set $\bar{e}^{\beta l} \simeq 1-\beta l$, $\bar{e}^{\delta l} \simeq 0$, and $|r| \ll 1$.

The acoustic signal then becomes

$$Q \simeq -i \frac{\beta u}{2a'} \left(\frac{u}{k}\right) Y \qquad (2.28)$$

The signal is proportional, in this case, to βu rather than βl. This indicats that only the light absorbed within the first thermal diffusion length contributes to Q, in spite of the fact that light is being absorbed throughout the length l of the solid. Also since $u < 1$, the thermal proporties of the backing material are replaced by those of the sample through the parameter (u/k). The frequency dependence of Q in this case is $\bar{w}^{3/2}$.

The previous three cases of optically thin solids demonstrate a unique capability of photo-acoustic spectroscopy of probing the depth profile of optical absorption within a sample . For materials with a high thermal diffusion coefficient "a" the probed surface layer can be as small as 0.1 um at chopping frequencies of $10^4 - 10^5$ Hz. Then by decreasing the chopping frequency, we increase the thermal diffusion length "u" and obtain optical absorption data further within the material, until at $\sim$5Hz we probe depths down to 10-100 um for materials

with high a-values and up to 1- 10 mm for materials with low a-values.

This capability for depth profile analysis is unique and opens up exciting possibilities in studying layered and amorphous materials and in determining overlay and thin film thicknesses.

2.3.2 Optically Opaque Solids ($l_\beta \ll 1$)

In these cases, most of the light is absorbed within a small distance compared to l, and essentially no light is transmitted.

Case 2a: Thermally Thin Solids ($\mu \gg l; \mu \gg l_\beta$).
In this case we set in (eq. 2.33) $\bar{e}^{\beta l} \simeq 0$, $e^{\pm \delta l} \simeq 1$, and $1r1 \gg 1$. We then obtain

$$ Q \simeq \frac{(1-i)}{2a'} \frac{(\mu'')}{k''} \gamma \qquad\qquad 2.39 $$

In this case our acoustic signal Q is independent of β. This applies to the case of a very black absorber such as carbon black. The signal is quite strong ($\frac{1}{\beta l}$ times stronger than case 1 a), depends on the thermal properties of the backing material, and varies as w^{-1}.

Case 2b: Thermally thick solids ($\mu < l; \mu > l_\beta$).
Here we set in (eq. 2.33) $\bar{e}^{\beta l} \simeq 0$, $\bar{e}^{\delta l} \simeq 0$, and $1r1 > 1$. We then obtain

$$Q \simeq \frac{Y}{2a'ak\beta}(\beta - 2a - i\beta) \simeq \left(\frac{1-i}{2a'}\right)\left(\frac{\mu}{k}\right)Y \qquad (2.40)$$

This is analegous to eq. 2.39 except the thermal proporties of the backing are replaced by those of the solid. Again Q is independent of β and varies as $\bar{w}^{-1}$.

Case 2c: Thermally Thick Solids $(\mu \ll 1; \mu < l_\beta)$.
We set $\bar{e}^{\beta l} \simeq 0$, $\bar{e}^{6l} \simeq 0$, and $lrl < 1$ in eq. 2.33.
We then obtain

$$Q = \frac{-i\beta Y}{4a'a^3k}(2a - \beta + i\beta) \simeq \frac{-i\beta \mu}{2a'}\left(\frac{\mu}{k}\right)Y \qquad (2.41)$$

This is a very interesting and important case. Although we are dealing here with a very optically opaque solid $(\beta l \gg 1)$ yet, as long as $\beta \mu < 1$ (i.e. $\mu < l_\beta$), the solid is not photoacoustically opaque and Q is proportional to β. As in case 1c, the signal is also dependent on the thermal properties of the sample and varies as $\bar{w}^{-3/2}$.

We shall apply, in chapter 4, the results of the present basic theory of photoacoustic spectroscopy in solids to the analysis of our experimental data on CdS.

Chapter 3

The Experimental Setup

Introduction

Figure 3.1 shows a block diagram of the experimental setup
which has been used for the measurement and recording of the
photoacoustic spectra. A dye laser pumped by an argon ion laser
provides a coherent tunable light source. The laser beam, after
bein modulated by a variable frequency rotating disc chopper, is
divided by a beam splitter into two beams. The first beam is
directed towards a photoacoustic cell which contains carbon pow-
der and acts as a power monitor for the dye laser when it is
scanned in wavelength by a clock motor attached to the laser
tuning mechanism. Its function depends on the fact that for a
very black absorber such as carbon black the thermal diffusion
length μ is much larger than the optical absorption path length
l_β (case 2a, chapter 2), and the photoacoustic signal is indepen-
dent of the optical absorption coefficient. In this case the
only term in eq. 2.39 that is dependent on the wavelength of the
incident radiation is the light source intensity I_o. Thus it
is clear that the photoacoustic spectrum in this case is simply
the power spectrum of the light source.

The second laser beam enters into a second identical
photoacoustic cell containing a powdered sample of cadmium sul-
phide (CdS). The two photoacoustic signals from the two photo-
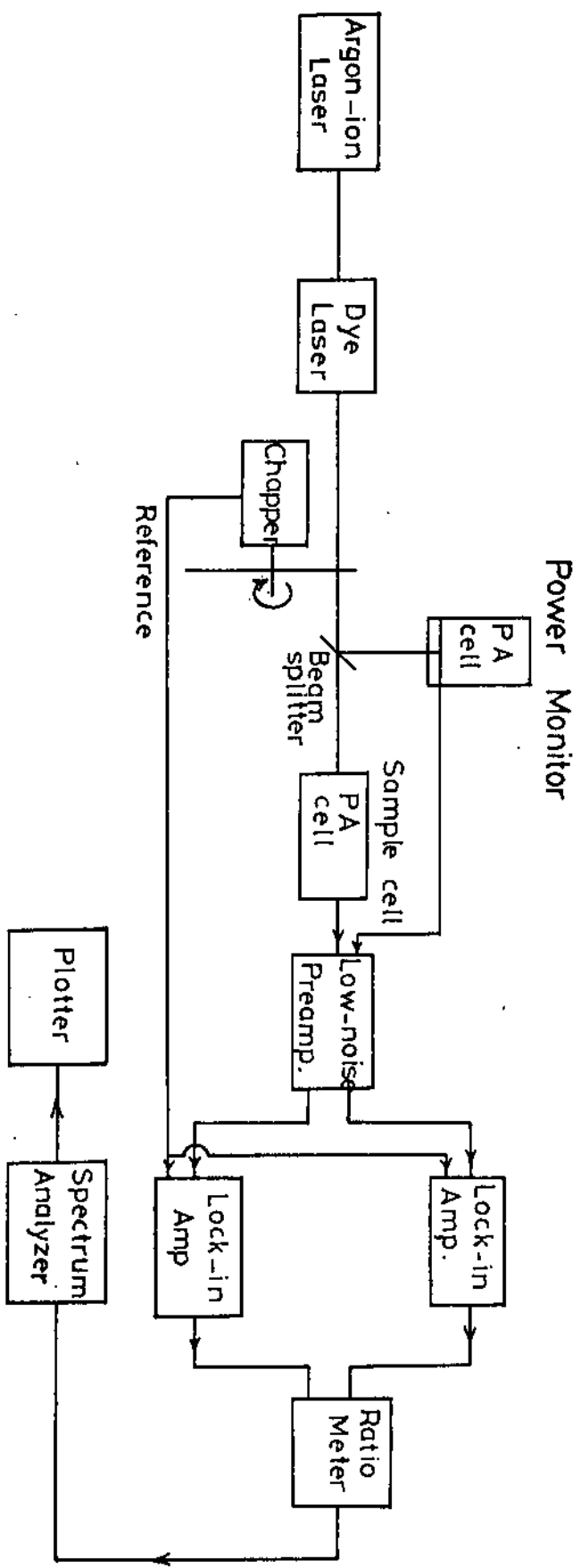acoustic cells are then amplified by two separate low noise

Fig 3.1 Block-Diagram of Experimental Set-up

preamplifers (see Apendix A). The resulting signals are then fed into two lock-in phase sensitive amplifiers. Both amplifiers are supplied by a reference signal from the chopper. The photoacoustic amplified signal of the CdS sample is then divided by the corresponding photoacoustic signal of the power monitor by an analog divider (see Apendix B). The normalized output spectrum of the ratio meter is now fed into a spectrum analyzer where it is stored and later recorded by the plotter.

We shall now give more specific details on the respective components of the previous experimental setup.

3.1 The Tunable Laser Source

An argon-ion laser (Spectra-Physics, Model 171) is used as a pump source for Spectra-Physics, Model 375 Tunable Dye Laser. The argon ion laser operates on population inversions in doubly ionized, singly ionized, and atomic argon that are excited by electrical discharge. Highly stable CW emissions occur at several UV wavelengths near 360 nm and at a dozen blue-green wavelengths in the 500 nm region. The argon ion laser is moderately efficient and the present high energy models are capable of producing about 4W in the ultraviolet and 20W in the blue-green region of the visible spectrum. It is worth mentioning that the gain in ion lasers is generally very strongly dependent on current density because such high densities are essential for maintaining a large population of ions in ionic states. In low-

current discharges, however, the atoms are primarily in excited states of the neutral atom. Secondly, the pwer output of ion lasers varies approximately as the square of the power input over a very large range of operating parameters. These properties result from the fact that the excitation process that generates the population inversion requires more than one collision step to reach the final upper state of the laser transition.

The model 171 Spectra-Physics argon ion laser utilizes power densities in excess of $5kW/cm^2$ in its plasma tube. The length of the laser cavity with the prism wavelength selector is 1.77 ± 0.003 meter with longitudinal mode separations of $\frac{c}{2L} = 84.7$ M H z. The Doppler-broadened argon ion gain profiles have bandwidths of more than 5000 M H z.

The dye laser is by far the most promising source of tunable coherent radiation in the UV-visible region. With the use of selected dyes, this laser can be continously tuned over the 340-1200 nm region with a spectral width of less than 1nm. Moreover, with the use of optical elements within the dye cavity, such as an etalon, linewidths of about 10^{-6} Å are attainable for ultra-high-resolution work. In addition to its role as a primary source of continously tunable narrow-band optical radiation, the dye laser can also be used to excite nonlinear devices that generate tunable coherent radiation as short as 100 nm. The tunability, spectral purity, and spatial coherence of dye lasers makes

them an excellent source for high resolution photoacoustic spectroscopy.

The model 375/376 laser system consists of Model 375 dye laser and Model 376 dye circulator. It is designed specifically to be pumped by an argon ion laser such as Spectra-Physics Model 171. The system is capable of producing tunable CW laser radiation at any wavelength from about 570 to 650 nm using a solution of Rhodamine 6G dye in ethylene glygol. By using other dyes, any wavelength from 440 to 915 nm may be obtained. Therefore the laser gain medium of the dye laser is a liquid solution of organic dye which absorbs pump laser light focused on it by the input mirror and emits light at longer wavelengths through fluorescence. This emitted light passes through the dye stream many times as it is reflected back and forth between the mirrors which form the optical cavity of the dye laser. As the light passes through the dye stream, dye molecules previously excited by the pump light are stimulated to emit at the fluorescence wavelengths, providing laser action. Fig. 3.2 shows the dye laser output spectrum profile for Rhodamine 6G. The fluorescent emission spectrum of the dye is typically a mirror image of the absorption spectrum displaced towards longer wavelengths. On the long wavelength side of the dye laser output, lasing is limited by the dye gain profile, and the shape of the dye laser output profile is approximately determined by the shape of the dye gain curve. On the short wavelength side, however, lasing
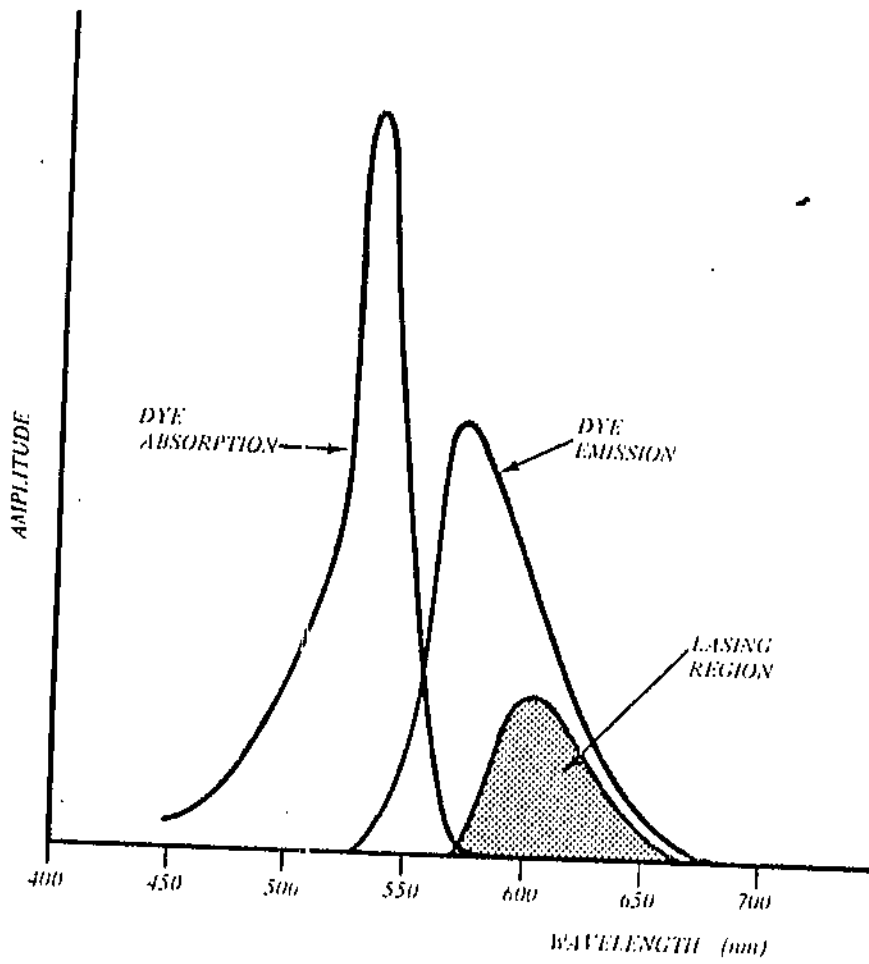
FIGURE 3.2 Rhodamine 6G Dye Characteristics

From Reference 19.

is limited by the absorption of the dye. Thus the dye laser output spectrum profile does not follow the shape of the dye gain curve in this area, but tapers off as the long wavelength tail of the absorption curve is reached.

The input mirror of the dye laser has a radius of curvature of 5cm and focuses the output beam of the pump laser into the dye stream, and is coated to provide maximum reflection at argon ion laser wavelengths. The laser has a three mirror folded optical cavity as shown in Fig. 3-3, with the "fold" occuring at the collimating mirror. The dye laser beam is reflected from the end mirror, through the dye stream, to the collimating mirror, to the output mirror and back again to complete one round trip as shown in the Figure. The standard end mirror and collimating mirror are identical. Both have a 5 cm radius of curvature and are coated to provide maximum reflection in the 600 nm wavelength region for use with Rhodamine 6G dye. The fluorescent spot of the dye is located at the center of curvature with respect to the end mirror and at the focus with respect to the collimating mirror. The output mirror is flat and is also coated for the same 600 nm wavelength region.

The length of the dye laser cavity between the extreme mirrors is about 36 cm with longitudinal mode separation of $\Delta V = \dfrac{c}{2L} = 400$ MHz. This mode separation is a result of the longitudinal resonance condition for any optical cavity,

$$L = n \frac{\lambda}{2}$$ or equivalently, $\nu = \frac{c}{\lambda} = n \frac{c}{2L}$ where n is an integer.

Wavelength tuning is accomplished by a highly selective Fabry-Perot tuning element shaped as a wedge and is inserted inside the dye laser cavity as shown in Fig. 3.3. The transmission of a Fabry-Perot etalon or etalon-like device such as the tuning wedge is given by the Airy formula. For a symmetrical lossless etalon with a reflectivity independent of wavelength, the formula reduces to

$$T = \frac{1}{1 + \frac{4r}{(1-r)^2} \sin^2 \phi}$$

where $\phi = 2 \pi n l_e \nu / c$, T is the transmittance, r is the coefficient of reflection, n is the index of refraction, l_e is the effective optical length of the cavity, c is the speed of light, and ν is the optical frequency. $T_{max} = 1$ and $T_{min} = \frac{(1-r)^2}{(1+r)^2}$ Fig.3.4 shows the transmission of an etalon-type device for various reflectivities. The frequency separation between two transmission maxima satisfying the resonance condition is called the free spectral range (FSR) = $\frac{c}{2nl_e}$.

Fig. 3.5 shows the construction of the tuning wedge with a FSR = 100,000 GHz = 110 nm. This is about the same as the width of the Rhodamine 6G dye gain curve. The wedge is
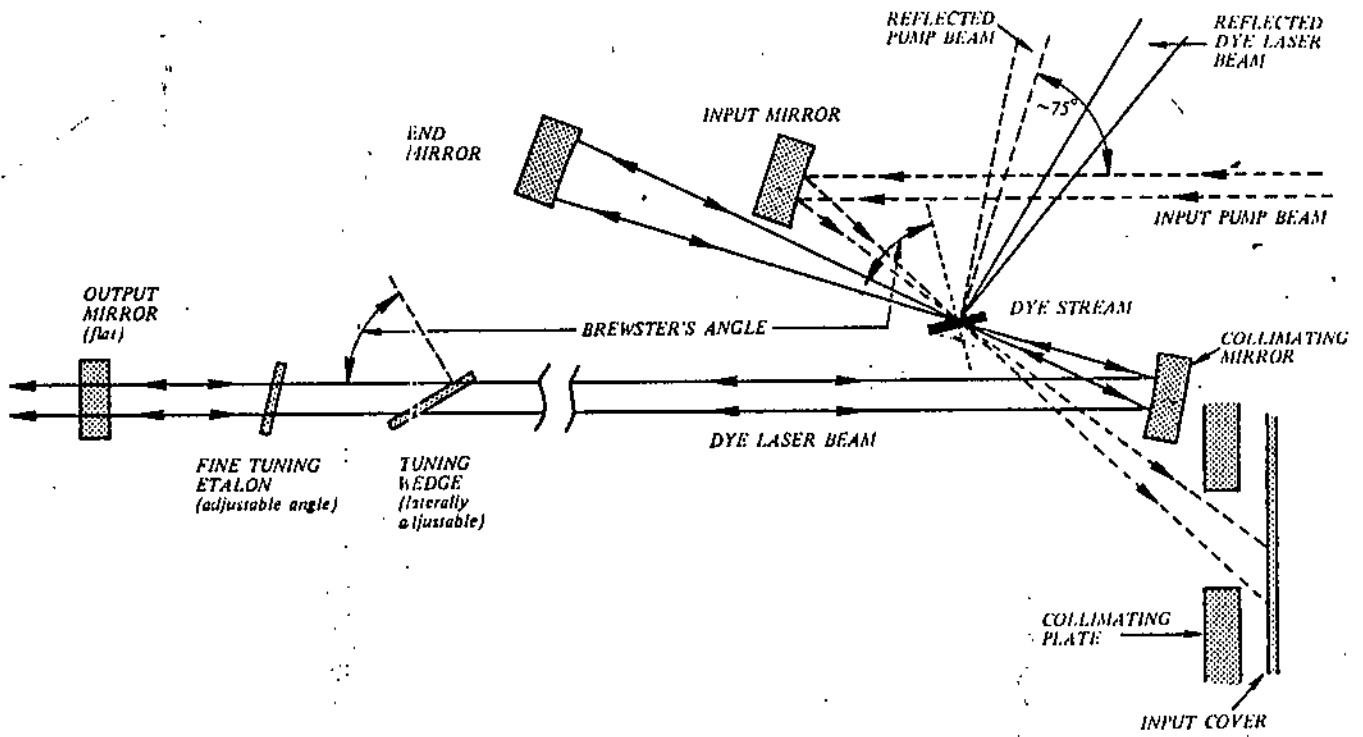
REFLECTED
PUMP BEAM

REFLECTED
DYE LASER
BEAM

INPUT MIRROR

END
MIRROR

~75°

INPUT PUMP BEAM

OUTPUT
MIRROR
(flat)

DYE STREAM

BREWSTER'S ANGLE

COLLIMATING
MIRROR

DYE LASER BEAM

FINE TUNING
ETALON
(adjustable angle)

TUNING
WEDGE
(laterally
adjustable)

COLLIMATING
PLATE

INPUT COVER

FIGURE 3.3 *Model 375 Dye Laser Optical System*

From Reference 19.
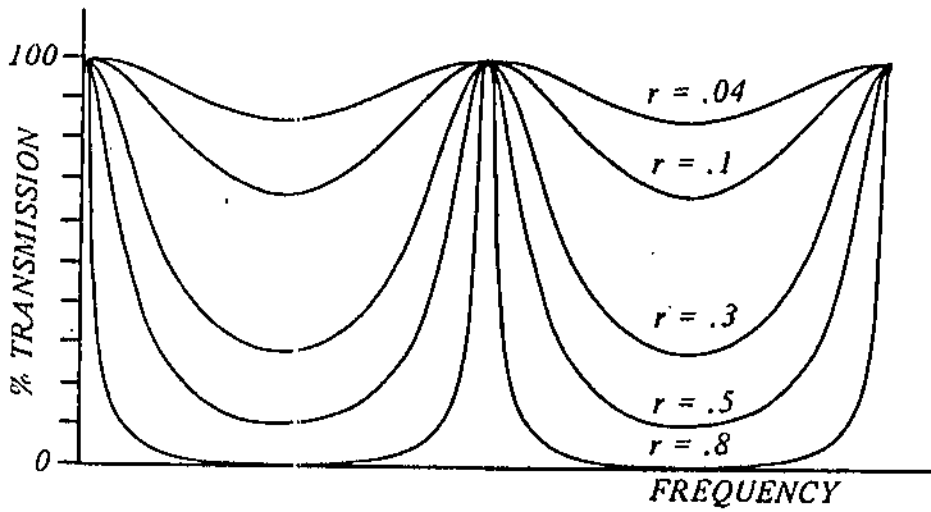
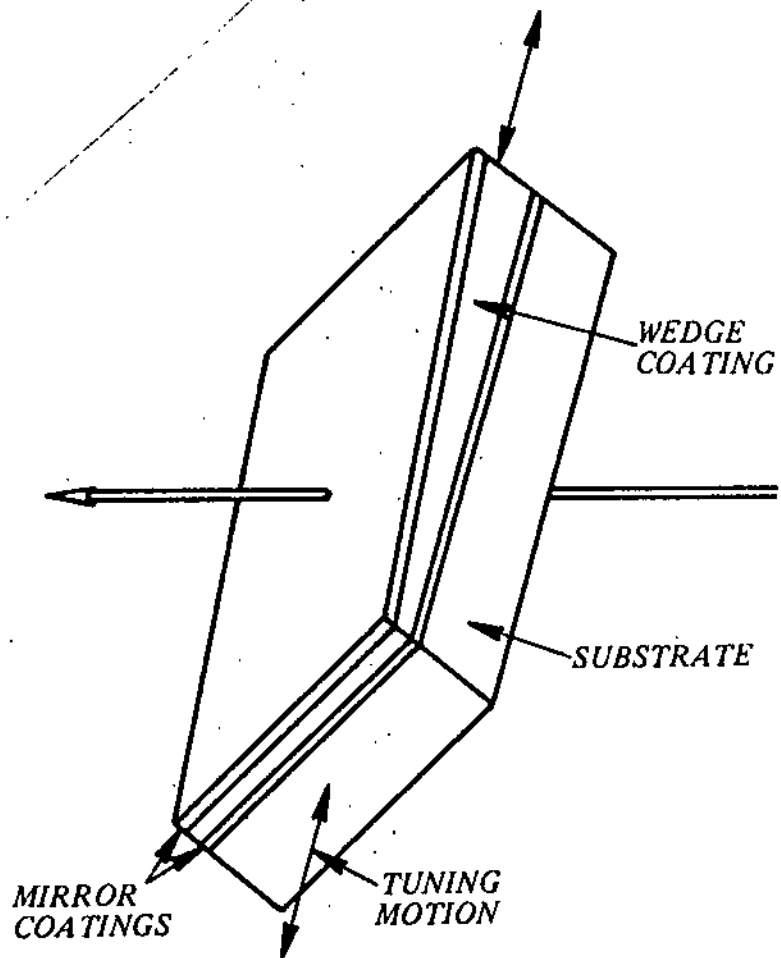FIGURE 3.4 Transmission for Various Reflectivities

From Reference 19.

WEDGE
COATING

SUBSTRATE

MIRROR
COATINGS

TUNING
MOTION

FIGURE 3.5 Tuning Wedge Construction

composed of very tin deposited layer of refractive index n
and variable length l_e with mirrors on either side. As the
wedge is moved laterally across the optical beam, the effec-
tive mirror spacing l_e changes, shifting the peak transmission
frequencies of the tuning wedge.

The output line width of the laser is mainly determined
by mode competition. To understand this process we note that
the dye gain curve of about 100 nm is wider than the cavity
axial mode spacing by at least a factor of 2×10^5 (see Fig.
3.6A). All these longitudinal modes lying under the dye gain
curve derive their energy from the same energy source-the dye
fluorescence transition. These modes can be considered as a
series of coupled oscillators at slightly different frequen-
cies. These coupling factors will result in competition, and
modes will tend to steal energy from one another. If for
example a mode is favored with respect to others by some gain/
loss mechanism it will increase in amplitude at the expense
of the others. The cavity modes near the peak of the dye gain
curve receive more of the energy pumped into the dye at the
expense of modes lying farther from the peak. Therefore, the
laser output, rather than being spread over a range of 100 nm,
it is concentrated within a range of about 2 nm (see Fig. 3.6B).

Similarly, with the tuning wedge inserted inside the cavi-
ty, the laser output is not the untuned output of Fig. 3.6B
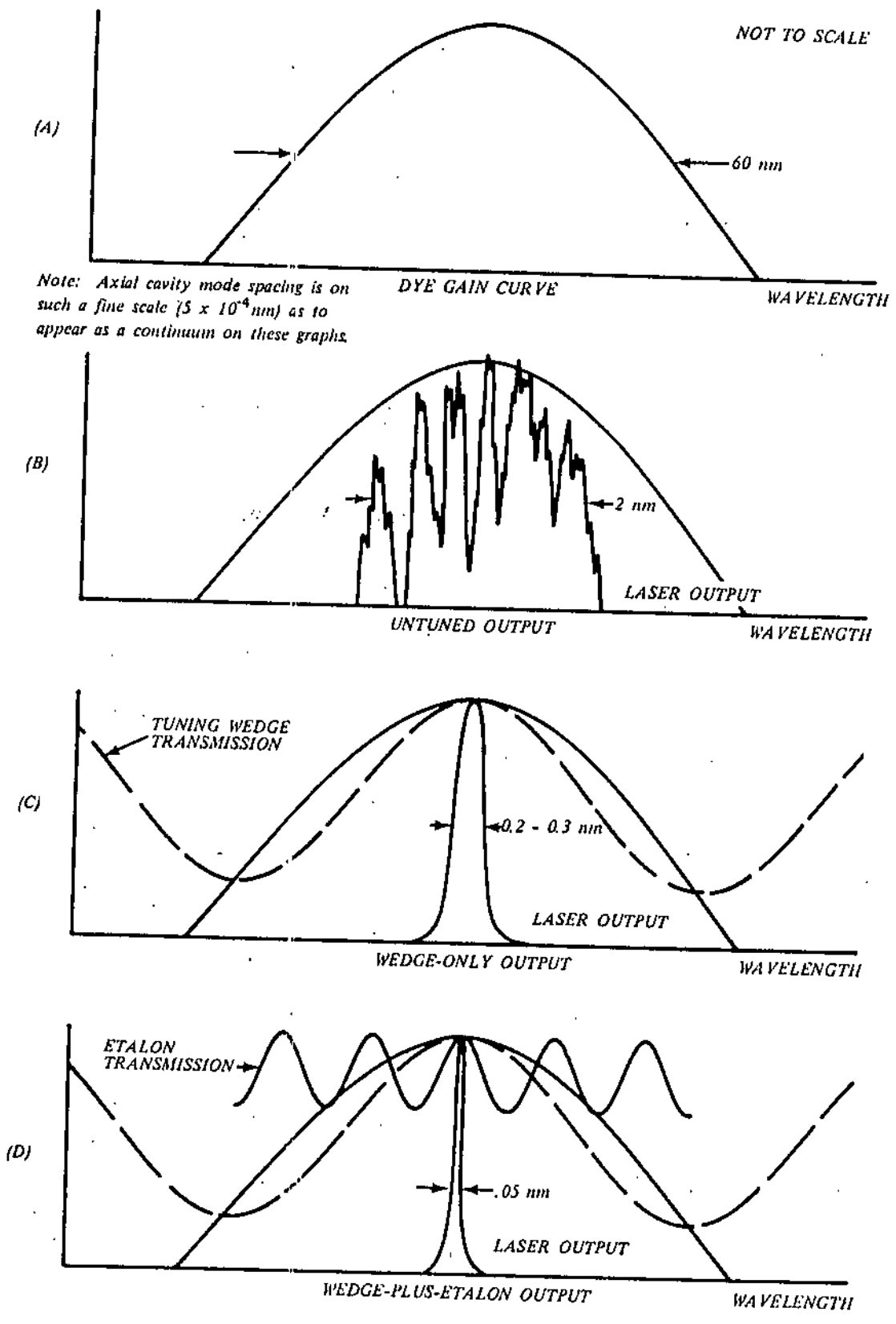modulated by the wedge transmission since mode competition

FIGURE 3.6 Mode Competition - Linewidth Narrowing

From Reference 19.

reduces the linewidth to 0.3 nm (see Fig. 3.6 C). Total output power does not decrease markedly, and thus the modes near the peak increase in power at the expense of those lying farther from the peak. The extra fine tuning etalon (see Fig. 3.3) will now further promote mode competition and narrows linewidth to 0.05 nm (see Fig. 3.6D). This last element is a thin uncoated piece of glass about 0.11mm thick and 900GHZ FSR. It acts as a transmission filter, allowing the laser to operate only at the resonance frequencies of the etalon, and thus provides coutinous wavelength tuning as it is tilted with respect to the dye laser beam.

Fig. 3.7 shows how the dye laser can be tuned with the tuning wedge alone. As the wedge is tuned, its transmission peak moves with respect to the dye gain curve (Figs. 3.7 A,B) and the output wavelength of the dye laser changes. The laser tunes continously across the gain curve of the dye as the wedge is moved laterally. Eventually, as the peak transmission frequency of the tuning wedge moves farther from the center of the dye gain curve, an adjacent tuning wedge transmission peak moves closer to the peak of the dye gain curve. At this point, the laser may be oscillating at two distinct wavelengths, separated by about 110 nm (Fig. 3.7c). As the wedge is moved a little farther (Fig. 3.7D) the laser no longer oscillates at the previous frequency, but now has an output only at the new frequency at the opposite side of the dye gain curve. If the

Labels in figure:

TUNING WEDGE TRANSMISSION

DYE GAIN CURVE

DYE LASER OUTPUT

(A)

AMPLITUDE

100,000 GHz (110 nm)

POSSIBLE OUTPUT FREQUENCIES BASED ON TUNING WEDGE TRANSMISSION

FREQUENCY

(B)

AMPLITUDE

FREQUENCY

(C)

AMPLITUDE

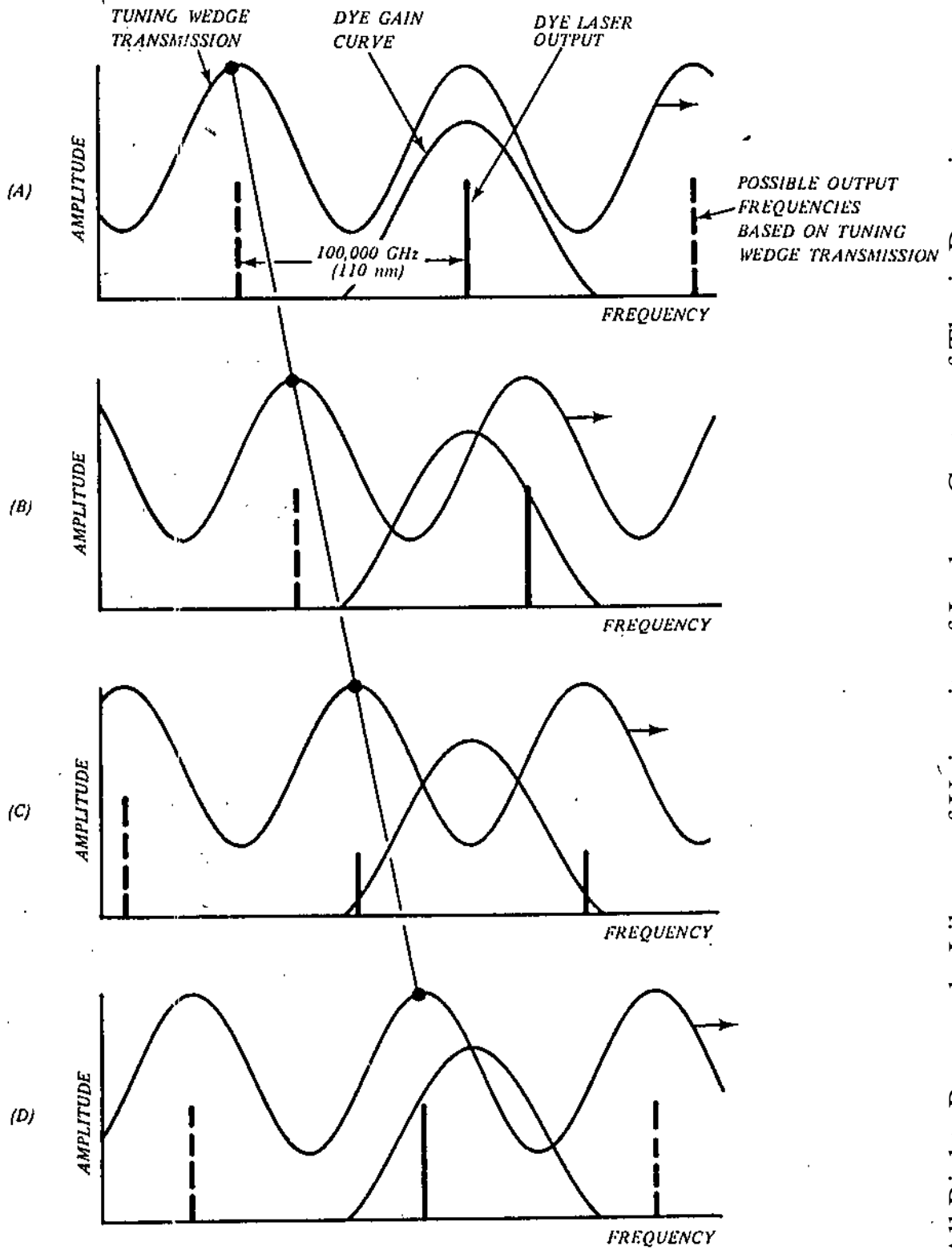FREQUENCY

(D)

AMPLITUDE

FREQUENCY

FIGURE 3.7 Dye Laser Tuning with Fine Tuning Etalon Removed

From Reference 19.

dye laser is operating at high power, this frequency hop occurs earlier than it did previously, and the frequency range over which the dye laser can be tuned is now less than it was at low power. This large output wavelength hop can be prevented if desired by using stops to limit the tuning wedge travel.

With both the tuning wedge and the fine tuning etalon in place, there are two ways to tune the laser—either with the wedge or with the etalon-as shown in Figs. 3.8 and 3.9 respectively. In this case, of course, the continous tuning range is limited to the free spectral range of the fine tuning etalon which is 1nm. Notice that the exact output wavelength is not determined strictly by the dye gain curve, the tuning wedge transmission curve, or the fine tuning etalon transmission curve. All three elements combine to determine the output wavelength, with the fine tuning etalon being most influential.

3.2 The Photoacoustic Cell-The Gas-Microphone Cell.

Figure 3.10 shows a schematic diagram of the photoacoustic cell for the gas-microphone PAS system which usually contains the sample and microphone. An electret microphone with internal self-biasing provided from a charged electret foil has been used in the present cell.
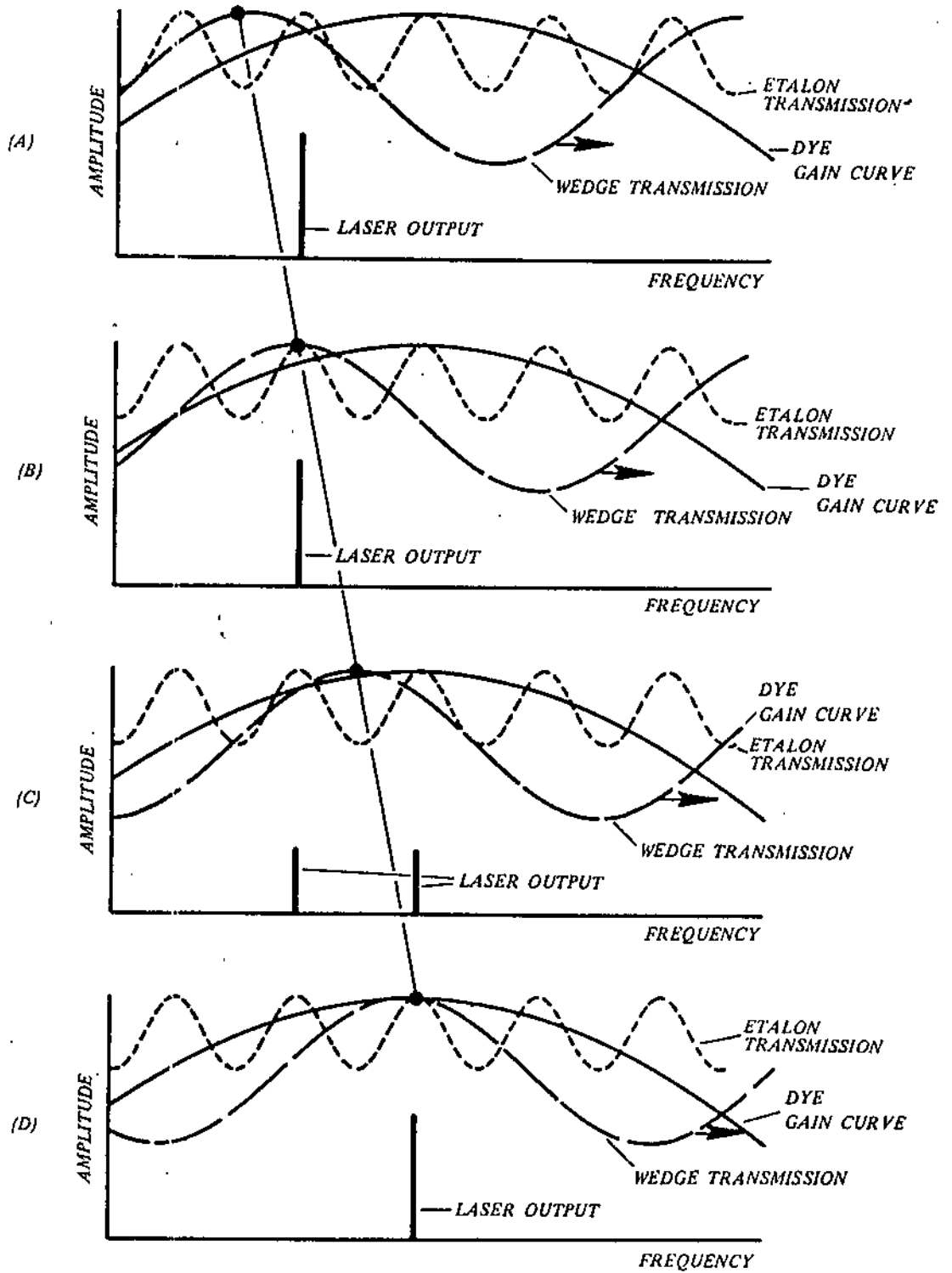
(A)
ETALON TRANSMISSION
DYE GAIN CURVE
WEDGE TRANSMISSION
LASER OUTPUT
AMPLITUDE
FREQUENCY

(B)
ETALON TRANSMISSION
DYE GAIN CURVE
WEDGE TRANSMISSION
LASER OUTPUT
AMPLITUDE
FREQUENCY

(C)
DYE GAIN CURVE
ETALON TRANSMISSION
WEDGE TRANSMISSION
LASER OUTPUT
AMPLITUDE
FREQUENCY

(D)
ETALON TRANSMISSION
DYE GAIN CURVE
WEDGE TRANSMISSION
LASER OUTPUT
AMPLITUDE
FREQUENCY

FIGURE 3.8 Tuning with the Wedge (Etalon Fixed)

From Reference 19.

(A)

AMPLITUDE

WEDGE
TRANSMISSION

ETALON TRANSMISSION

DYE
GAIN CURVE

LASER OUTPUT

FREQUENCY

(B)

AMPLITUDE

WEDGE
TRANSMISSION

ETALON TRANSMISSION

DYE
GAIN CURVE

LASER OUTPUT

FREQUENCY

(C)

AMPLITUDE

WEDGE
TRANSMISSION

DYE
GAIN CURVE

ETALON TRANSMISSION

LASER OUTPUT

FREQUENCY

(D)

AMPLITUDE

WEDGE
TRANSMISSION

ETALON TRANSMISSION

DYE
GAIN CURVE

LASER OUTPUT

FREQUENCY

FIGURE 3.9 Fine Tuning with the Etalon (Wedge Fixed)

From Reference 19.
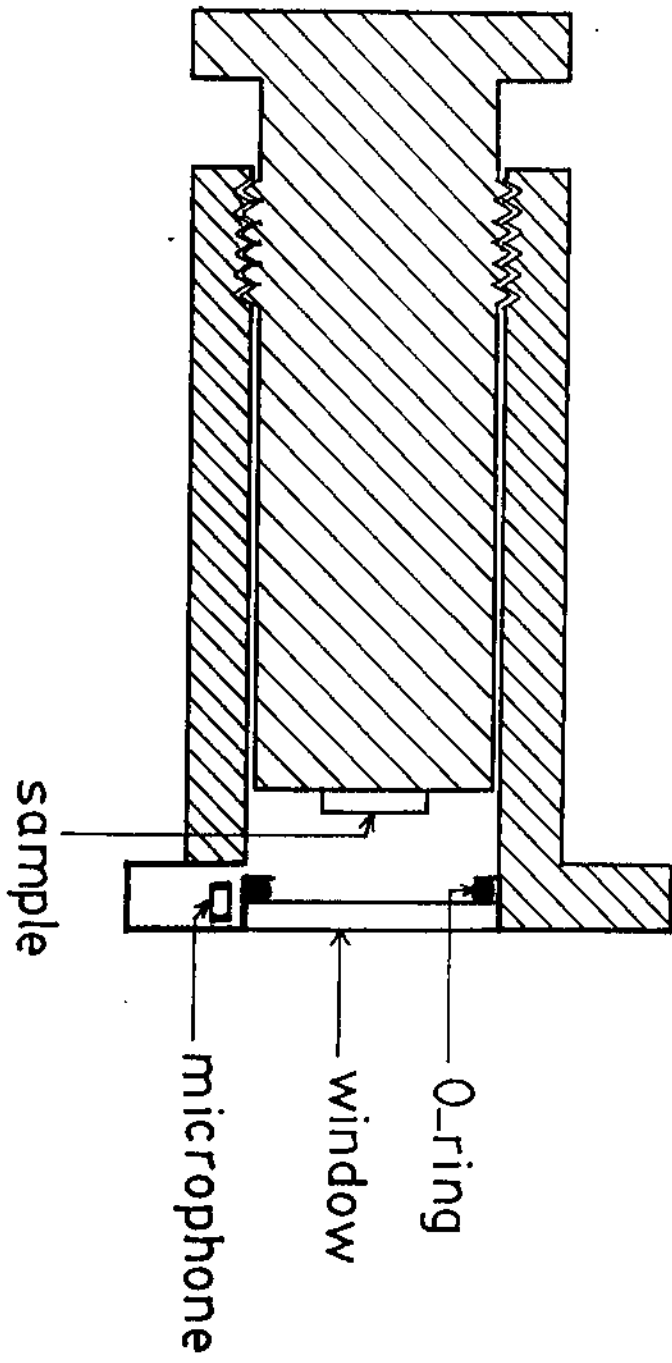
Fig 3.10 Photoacoustic Cell

sample

microphone

window

O-ring

In designing a photoacoustic cell, one has to consider the following relevant criteria:

1. Acoustic isolation from the outside world.

2. Minimizing extraneous photoacoustic signals arising from the interaction of the light beam with the walls, the windows, and the microphone in the cell.

3. Microphone configuration.

4. Means for maximizing the acoustic signal within the cell.

5. Restrictions imposed by the samples to be studied and the type of experiment to be performed.

We shall now consider the previous criteria in some more detail.

Acoustic isolation does not impose a serious problem provided one uses lock-in detection methods for analyzing the photoacoustic signal. One should avoid, however, using chopping frequencies close to those present in the acoustic and vibrational spectrum of the environment. The design should have good acoustic seals and thick walls which form an efficient acoustic barrier. In addition, some isolation of the cell from room vibrations should also be considered.

To minimize the photoacoustic signal arising from the interaction of the light beam with the windows and walls of the cell, one should use windows which are as optically transparent as possible for the wavelength region of interest, and

construct the body of the cell out of thick polished metal such as aluminium, brass, or stainless steel. A large polished thermal mass results in little absorption of light with subsequent small temperature rise at the surface and a small photoacoustic signal. One should also keep all inside surfaces clean to minimize photoacoustic signals from surface contamination. Finally the design should consider minimizing the amount of scattered light that can reach the microphone diaphragm.

The microphone used for the cell of Fig. 3.10 is a cylindrical small electret microphone 1cm in diameter and 1.0 cm long. Such microphones have rated sensitivity of about 1mV/μbar, with a flat frequency response from about 50Hz to 15kHz. The photoacoustic signals from the microphones were first preamplified by a locally built low noise preamplifier before being fed to the lock-in amplifiers. With a carbon black absorber the photoacoustic signal was about 20mV at 790 Hz for the incident laser light at 5980 $\overset{o}{A}$. The signal to noise ratio for the carbon-black absorber was about 500:1. The noise is mainly electronic due to the microphone-preamplifier system.

Since the signal in a photoacoustic cell used for solid samples varies inversely with l' (eq. 2.33), one should minimize the gas volume provided that the distance l' between the sample and the cell window should always be greater than the thermal diffusion length u' of the gas. This results from

the fact this boundary layer of the gas acts as an acoustic piston generating the signal in the cell, and when $l \lesssim u'$, the photoacoustic signal decreases. Now since $u' \propto (w)^{-\frac{1}{2}}$ we should keep $l' > u'$ for the lowest chopping frequencies used. For air at room temperature and pressure $u' = 0.06 \text{cm}$ at 10Hz. A reasonable value for l' would then be about 0.1 cm. At higher frequencies thermoviscous damping becomes predominant resulting in an attenuation e^{-Ex}, where E is a damping coefficient given by[15],

$$ E = \frac{1}{dc_0} \left(\frac{n_e w}{2 \rho_0} \right)^{\frac{1}{2}} $$

where d is the closest dimension between cell boundaries, as in a passageway, c_0 is the sound velocity, ρ_0 is the gas density, and n_e is the effective viscosity which depends on both the ordinary viscosity and thermal conductivity of the gas. Again for air at room temperature and pressure, thermoviscous damping is negligible at 100Hz if $d > 0.01 \text{cm}$. In general it is better to keep any passageway dimension between 1-2 mm.

The limit to which one adheres to the previous criteria depends on the type of sample used (powder, smear, liquid etc.), its size, and the type of experiment one wishes to perform.

Chapter 4

EXPERIMENTAL RESULTS AND CONCLUSIONS

4.1 The Power Spectrum of The Dye Laser.

In this chapter we shall consider some of the predictions of the Rosencwaig-Gersho theory of the photoacoustic effect in solids which we detailed in Chapater 2, and shall show how these predictions could explain our experimental results.

We shall begin with the most important and obvious results of the theory which indicates (see eq. 2.33) that the photoacoustic signal is always linearly proportional to the incident light power for any sample or cell geometry. However we have seen (eqs. 2.39 and 2.40) that in the special cases when the thermal diffusion length in an optically opaque sample is greater than the optical absorption length $(\mu > l_B)$, the photoacoustic signal is independent of the optical absorption coefficient B of the sample. In these special cases, the only wavelength dependent parameter in eqs. 2.39 and 2.40 is the light source intensity I_o, and the photoacoustic spectrum in these cases is simply the power spectrum of the light source.

Fig. 4.1 shows the power spectrum of the dye laser as indicated experimentally by the photoacoustic spectrum of a porous carbon powder sample. The laser was scanned over the wavelength range from 5727 $\overset{o}{A}$ to 6352 $\overset{o}{A}$; and the spectrum
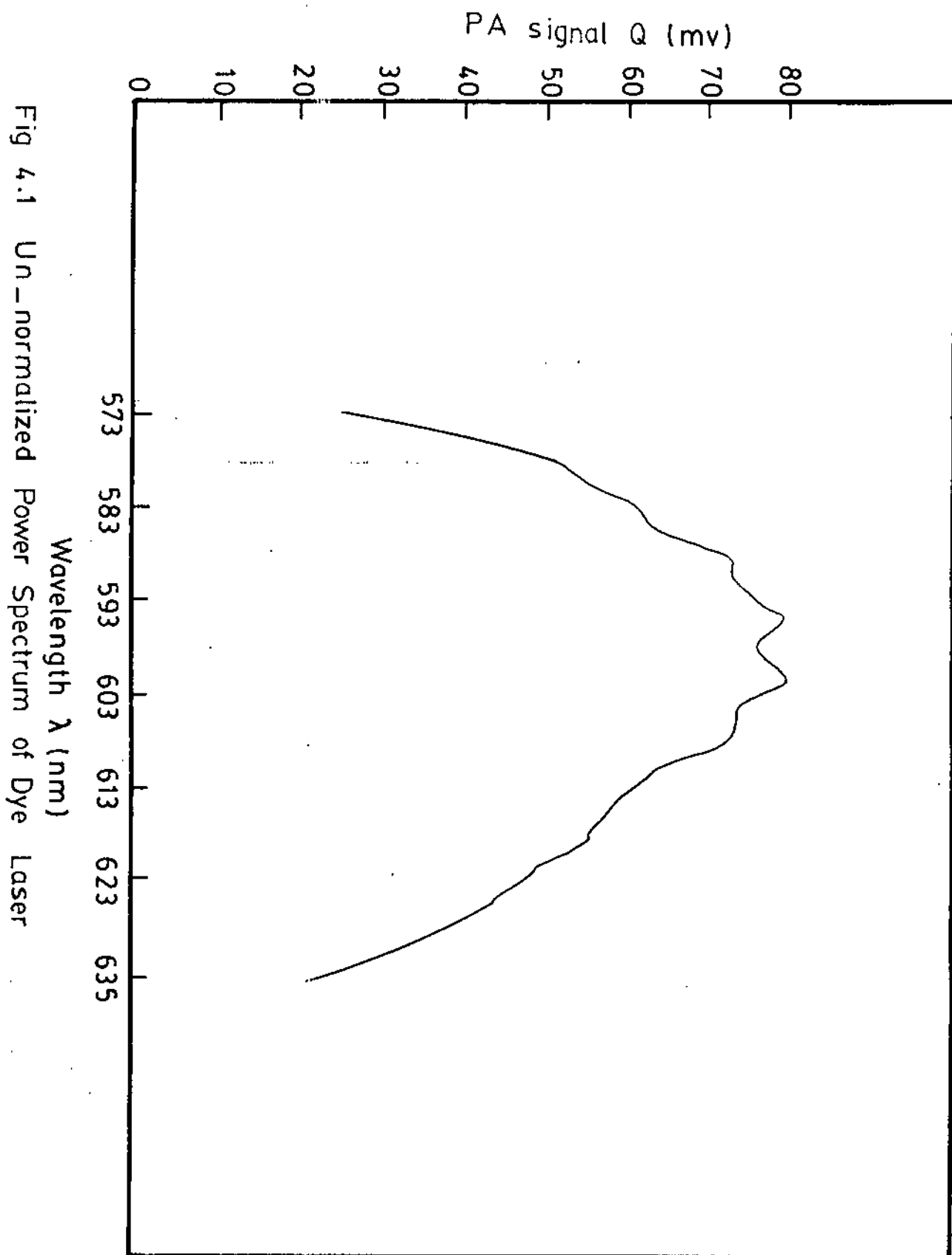
Fig 4.1 Un_normalized Power Spectrum of Dye Laser

indicates the large intensity fluctuations of the laser power over the respective range of tuning. It should be mentioned in this respect that one can utilize this property of the photoacoustic spectrum in constructing a power meter that would have a greater wavelength range than other available power meters[5], while maintaing high sensitivity and a fairly large dynamic range. The same power meter could be used from the X-ray range to the far infrared, requiring only a change of entrance window to allow suitable transmission of the incident radiation.

4.2 Normalization of the Power Spectrum of the Dye Laser.

To overcome the intensity fluctuations of the dye laser power spectrum of Fig. 4.1 a photoacoustic cell containing carbon powder was used as a power monitor (see Fig. 3.1). Normalized PA spectra are then obtained by dividing the photoacoustic signal of the sample by the signal of the power monitor using an analog divider (see Appendix B).

To test the efficiency of the previous normalization procedure the power spectrum of the dye laser of Fig. 4.1 was normalized and the experimental result is demonstrated in Fig. 4.2. The resulting intensity fluctuations of the dye laser power as measured by the ratio $(I_{max} - I_{min})/I_{av}$ over the entire tuning range of the dye does not exceed 6% compared with 200% before normalization.
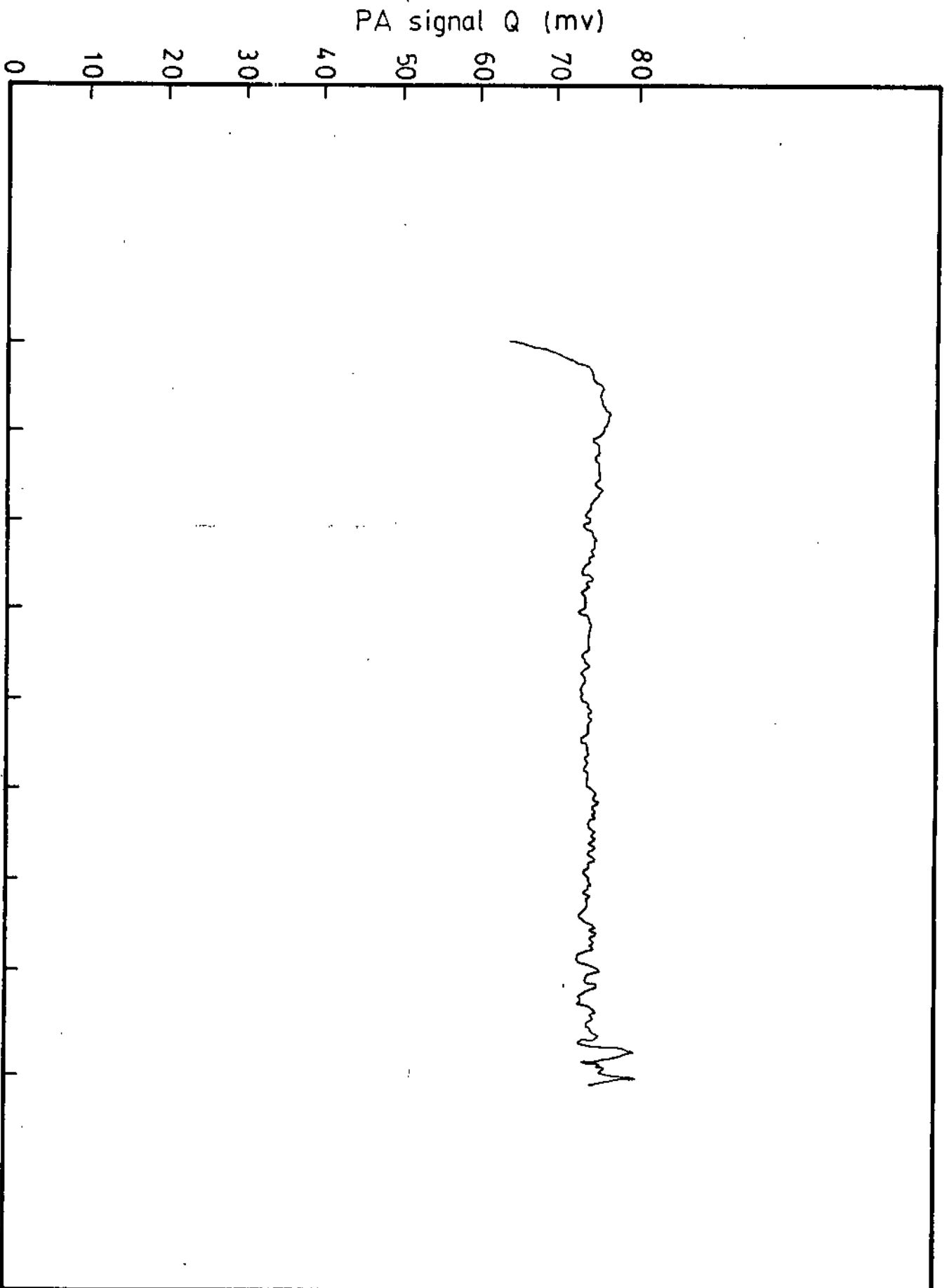
Fig 4.2 Normalized Power Spectrum of Dye Laser

4.3   Variation of The Photoacoustic Signal with Frequency.

The Rosencwaig-Gersho theory of the photoacoustic effect has made certain predictions about the variation of the photoacoustic signal with the modulation frequency. These predictions depend on the thermo-optical properties of the investigated sample.

4.3.1   The Case of Carbon Black.

We have seen that carbon black is characterized by its photoacoustic "opaqueness" as well as its optical opaqueness, in the sense that the acoustic signal is independent of the optical absorption coefficient B, and is given by (see Eq. 2.39)

$$Q \simeq \frac{1-i}{2a'} \left(\frac{u''}{k''} \right) Y$$

To find the frequency dependence of Q we substitute for a' and u'' where $a' = \left(\frac{w}{2\alpha'} \right)^{\frac{1}{2}}$ and $u'' = \left(\frac{2\alpha''}{w} \right)^{\frac{1}{2}}$, and we get

$$Q \simeq \frac{(1-i)}{k''} \frac{\sqrt{\alpha'\alpha''}}{w} Y$$

which indicates that Q varies as w^{-1} i.e. a log-log graph of Q versus the modulation frequency f would give a straight line of slope -1.

Fig. 4.3 shows the experimental plot of log Q against log f for carbon black. The slope of the best fit straight line to the experimental data points is equal to -1 as
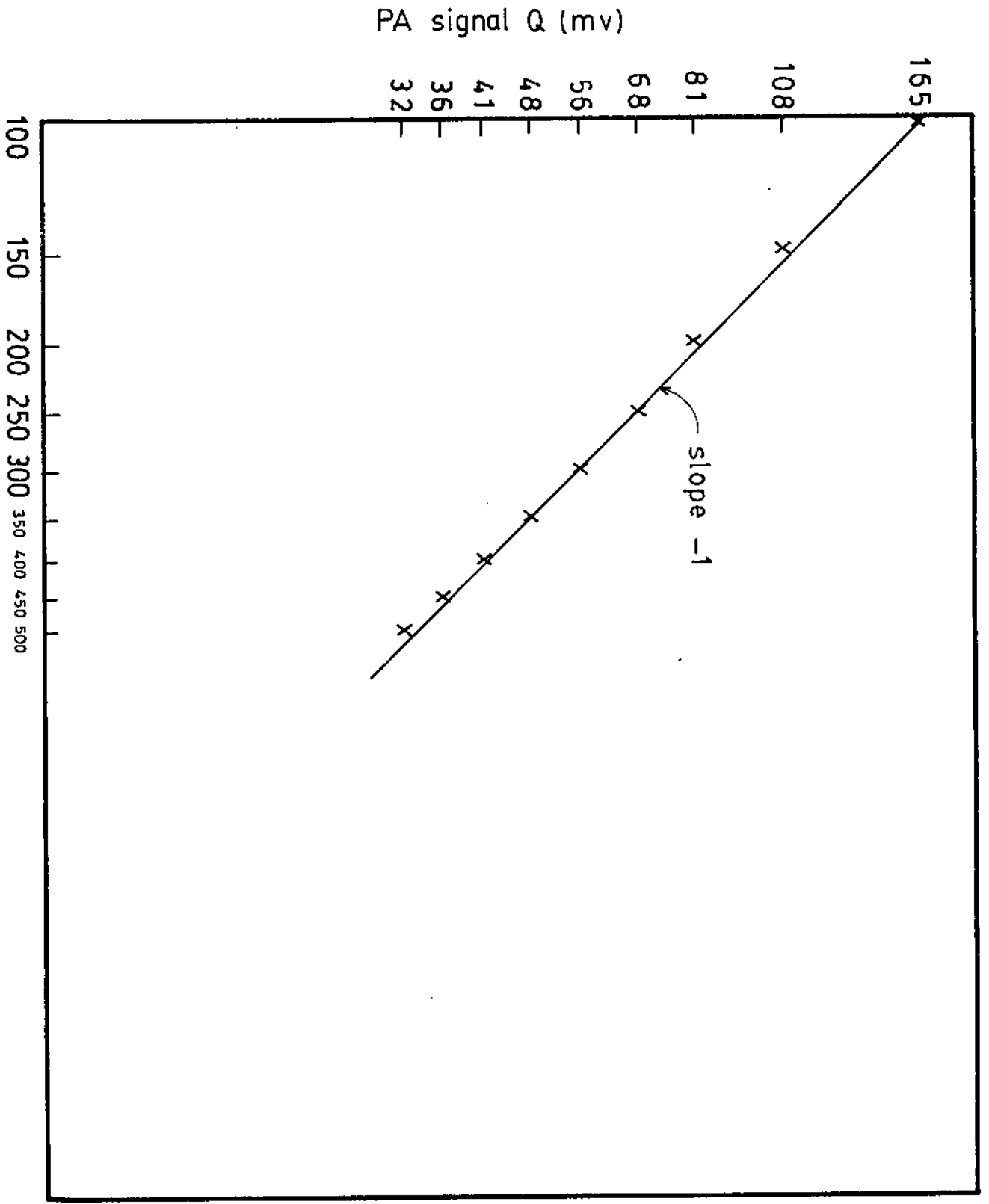
Fig 4.3 Variation of PA signal of Carbon black with Frequency

predicted by the RG   theory.

4.3.2   The Case of Cadmium Sulphide.

To study the variation of the PA   signal   Q with frequency f for a sample cadmium sulphide, a sample of   CdS   in powder form was used. The experimental graph of log Q against log f is shown in Fig. 4.4.

To understand the nature of the dependence of the PA signal Q on the modulation frequency f as demonstrated in Fig. 4.4 we note that CdS is an optically opaque solid with $l_B < 1$, in the sense that most of the light is absorbed within a distance that is small compared to the length of the sample 1 such that essentially no light is transmitted. For such materials we have to differentiate between two situations. The first one occurs in the low frequency domain where $u > l_B$, i.e. the thermal diffusion length u is greater than the optical path length l_B. We have seen in Chapter 2 that for such thermally thick solids Eq. 2.39 shows that

$$Q \cong \frac{1-i}{2a'} \left(\frac{u}{k} \right) Y$$

and with $u = \left(\frac{2\alpha}{w} \right)^{\frac{1}{2}}$, $a' = \left(\frac{w}{2\alpha'} \right)^{\frac{1}{2}}$ we get

$$Q \cong \frac{1-i}{k} \frac{\sqrt{\alpha\alpha'}}{w} Y$$

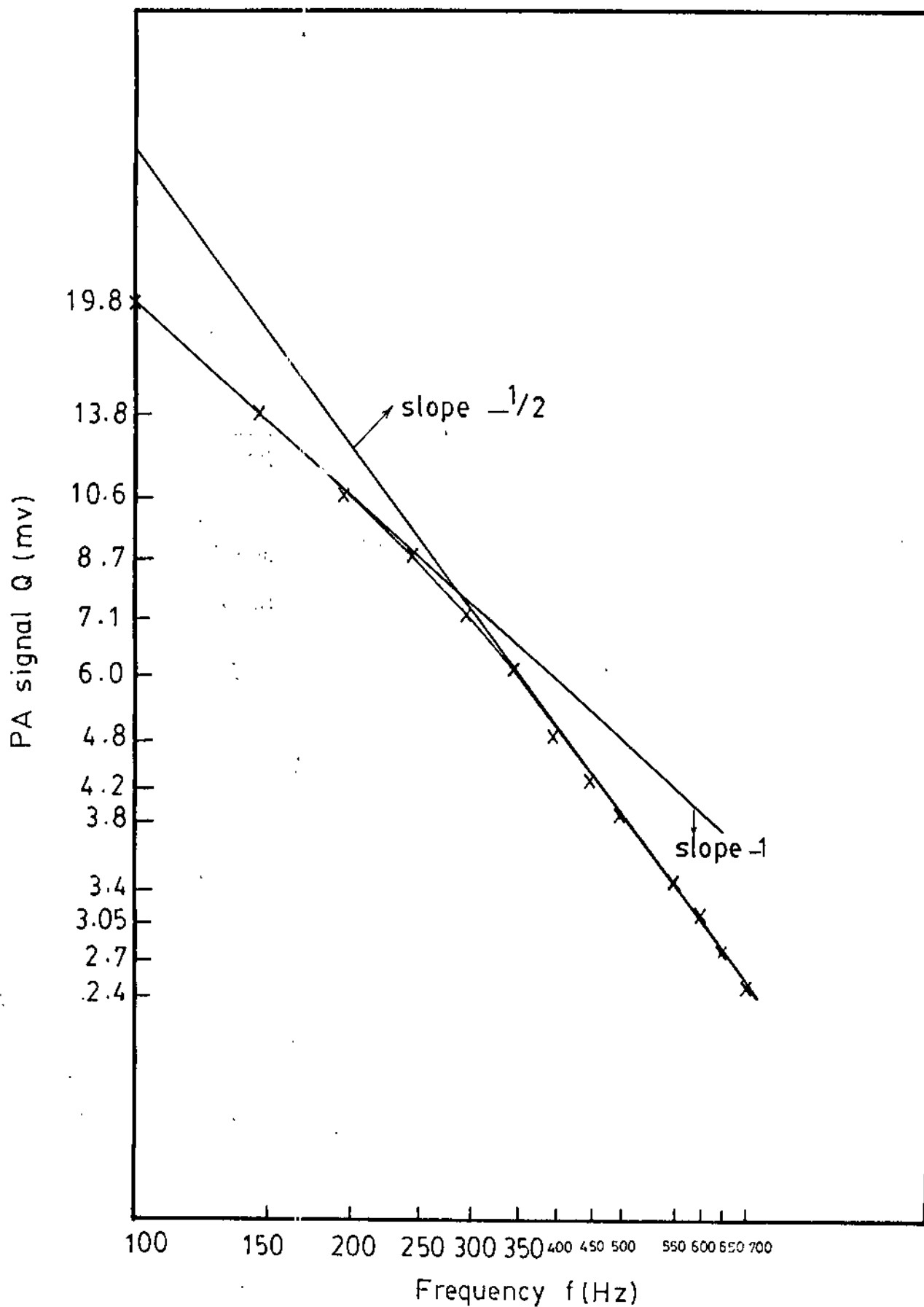which shows that in the low frequency range where $u > l_B$, the

Fig 4.4 Variation of PA signal of Cadmium sulphide (CdS) with Frequency

PA signal Q varies as w^{-1} i.e. a plot of log Q versus log f gives a straight line with slope -1.

Now with continous increase in the modulation frequency f, a stage is reached when u, which varies as $w^{-\frac{1}{2}}$ becomes smaller than the optical path length l_B. In this case the PA signal Q, as Eq. 2.40 indicates, becomes equal to

$$Q \approx \frac{-iBu}{2a'} \left(\frac{u}{k} \right) Y$$

and with $a' = \left(\frac{w}{2\alpha'} \right)^{\frac{1}{2}}$, $u = \left(\frac{2\alpha}{w} \right)^{\frac{1}{2}}$ we get

$$Q \approx \frac{-iB}{k} \sqrt{2\alpha'} \frac{\alpha}{w^{3/2}}$$

which indicates that Q varies as $w^{-3/2}$, i.e. a plot of log Q against log w gives a straight line with a slope of $-3/2$.

Looking back now on the experimental graph of Fig. 4.4 we indeed observe that by varying the chopping frequency we move from a region of w^{-1} dependence with a slope of -1 for the log-log curve to another region of $w^{-3/2}$ dependence with a slope of $-\frac{3}{2}$ for the log-log curve as shown in Fig. 4.4. The transition between these two regions occurs for CdS around f = 400 Hz. At this transition frequency $u = l_B$. Now $u = \left(\frac{2\alpha}{w} \right)^{\frac{1}{2}}$ where $\alpha = \frac{k}{\rho C}$. For CdS.

$$k = 0.2 \text{ watt } (\text{cm. K})^{-1}$$

$$\rho = 4.8 \text{ g.cm}^{-3}$$

$$C = 0.33 \text{ Joule } (\text{g.K})^{-1}$$

Substituting for these values we get

$$\alpha \simeq 0.15 \ (\text{cm}^2/\text{sec})$$

Now at $f = 400$ Hz and $\alpha \simeq 0.15$ cm^2. sec^{-1} we get for the thermal diffusion length u at this frequency,

$$u = \left(\frac{2 \times 0.15}{2 \times 3.14 \times 400} \right)^{\frac{1}{2}} \simeq 0.011 \text{ cm}$$

We conclude from this that at $f = 400$ Hz we have $u = l_B = 0.011$ cm, and with $l_B = \frac{1}{B}$ we find that $B = 91.3 \text{ cm}^{-1}$ at $\lambda = 593$ nm. This is the dye laser wavelength at which the data were taken.

4.4 The Normalized Absorption Spectrum of CdS.

Fig. 4.5 shows the normalized photoacoustic signal of cadmium sulphide CdS at room temperature over the wavelength range 571-635.5 nm of the dye laser. Our results agree reasonably well with those of other workers[16,17]. Cadmium sulphide is a direct-band semiconductor with the band edge as measured by the position of the knee in the PAS spectra at $\lambda = 518.1$ nm (2.4eV) was found to agree very well with the values recorded in the literature[18]. Unfortunately the

tunability of our dye laser using Rhodamine 6G dye does not cover the previous wavelength.

Several remarks of PAS spectra of semiconductors are in place at this point. First the photoacoustic spectroscopy technique gives the correct spectrum for both direct (CdS) and indirect (GaP) bandgap semiconductors. Second the samples can be in the form of commercially available powders taken off the shelf without further purification or of single crystals ground up to powder form to reduce reflectivity and increase the surface area. Third, the quantity needed may not exceed a few milligrams. Finally the relative simplicity of the experimental technique used. All of this emphasizes the ease and convenience with which data of importance for the optical and electrical properties of semiconductors may be obtained without the requirements of high purification or high vacuum techniques.

4.5 The Variation of The Absorptivity B of CdS with Wavelength.

Fig. 4.5 of the PA spectrum of CdS could be transformed into the corresponding variation of the optical absorption coefficient of CdS with wavelength over the tunability range of the dye laser. Using the calculated value of B = 91.3 cm^{-1} at λ = 593 nm (see sec. 4.3.2) we computed the corresponding variation of B with wavelength as shown in Fig. 4.6.

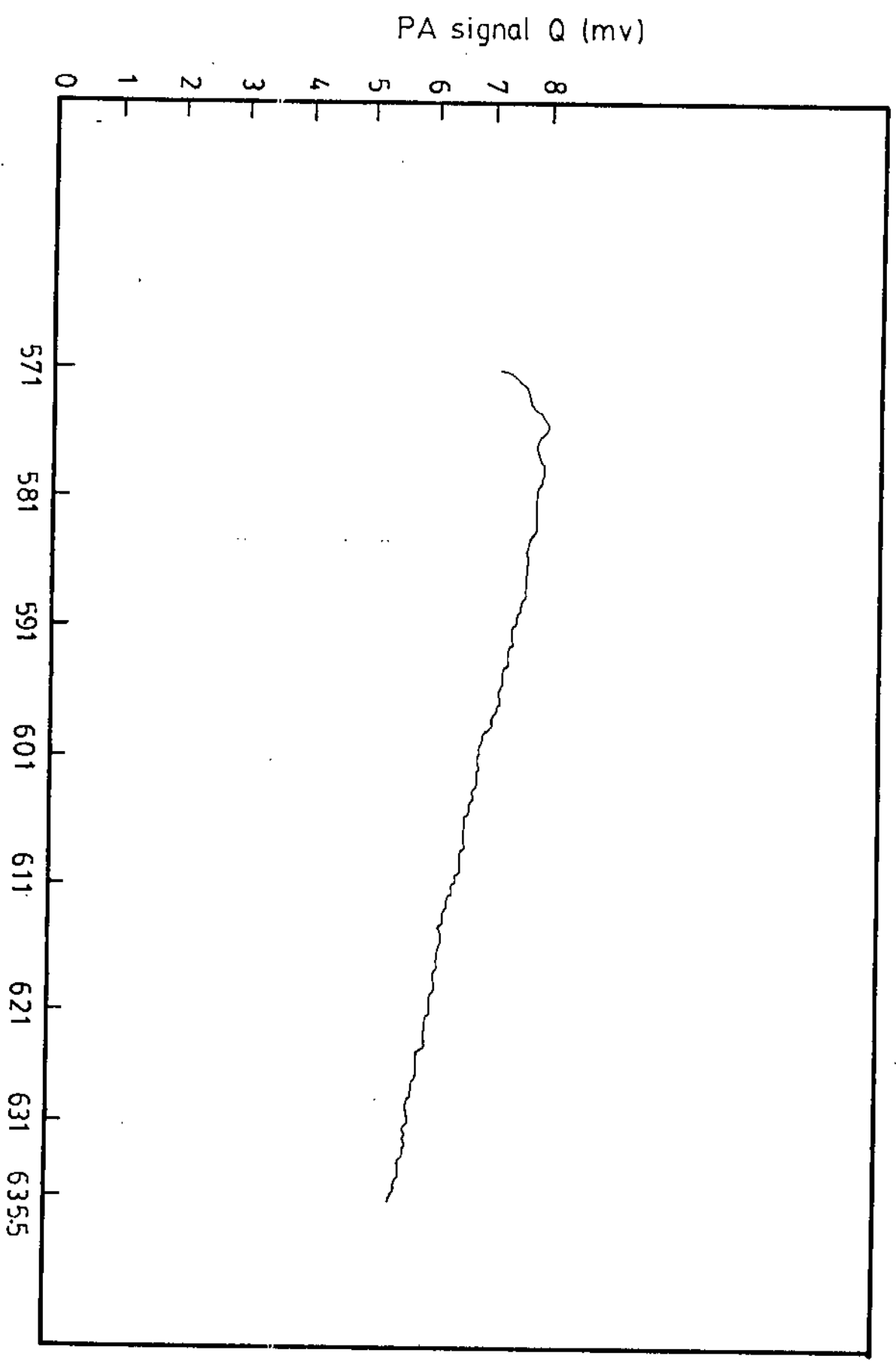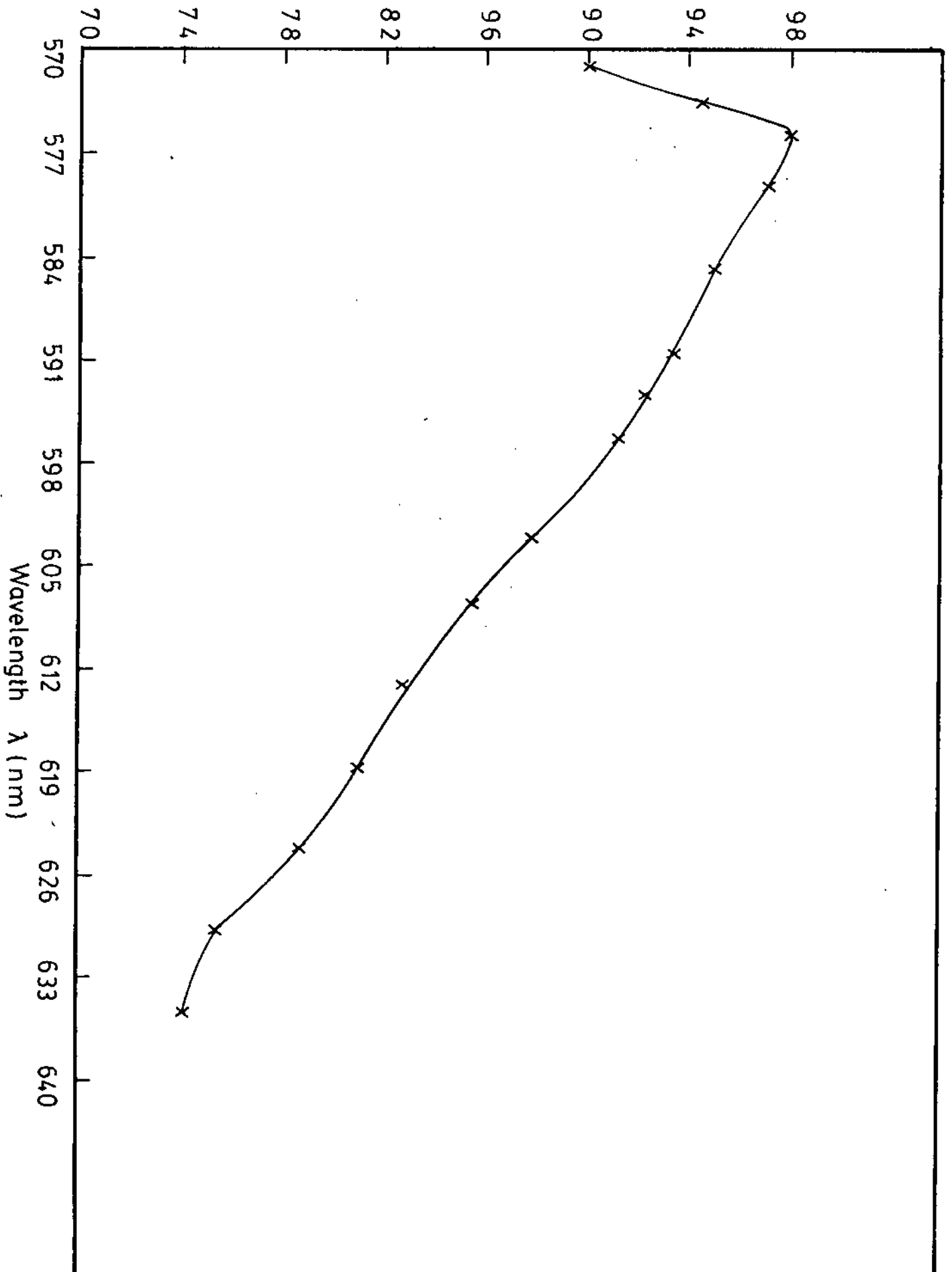Fig 4.5   Normalized PA signal of Cadmium Sulphide (CdS) with Dye Laser wavelength

Fig 4.6 Variation of the Absorption Coefficient β of Cadmium Sulphide (CdS) with wavelength

4.6 Conclusions.

During the course of this work we succeeded in building a complete experimental setup for Laser Photoacoustic Spectroscopy, including building up necessary mechanical and electronic components at the Department's workshops.

The setup was tested and its performance was evaluated in the light of the Rosencwaig-Gersho (RG) theory of photoacoustic spectroscopy in condensed media.

The photoacoustic spectrum of CdS both as a function of modulating frequency for a fixed wavelength and as a function of wavelength for a fixed frequency were obtained. The log-log curve of the photoacoustic signal with frequency was explained in the light of the RG-theory and the difference in the frequency dependence was explained in terms of the relative values of the thermal diffusion length u and the optical path length l_B. The overlap region between the two frequency domains was determined and a value of $B = 91.3$ cm^{-1} for CdS at $\lambda = 593$ nm was calculated.
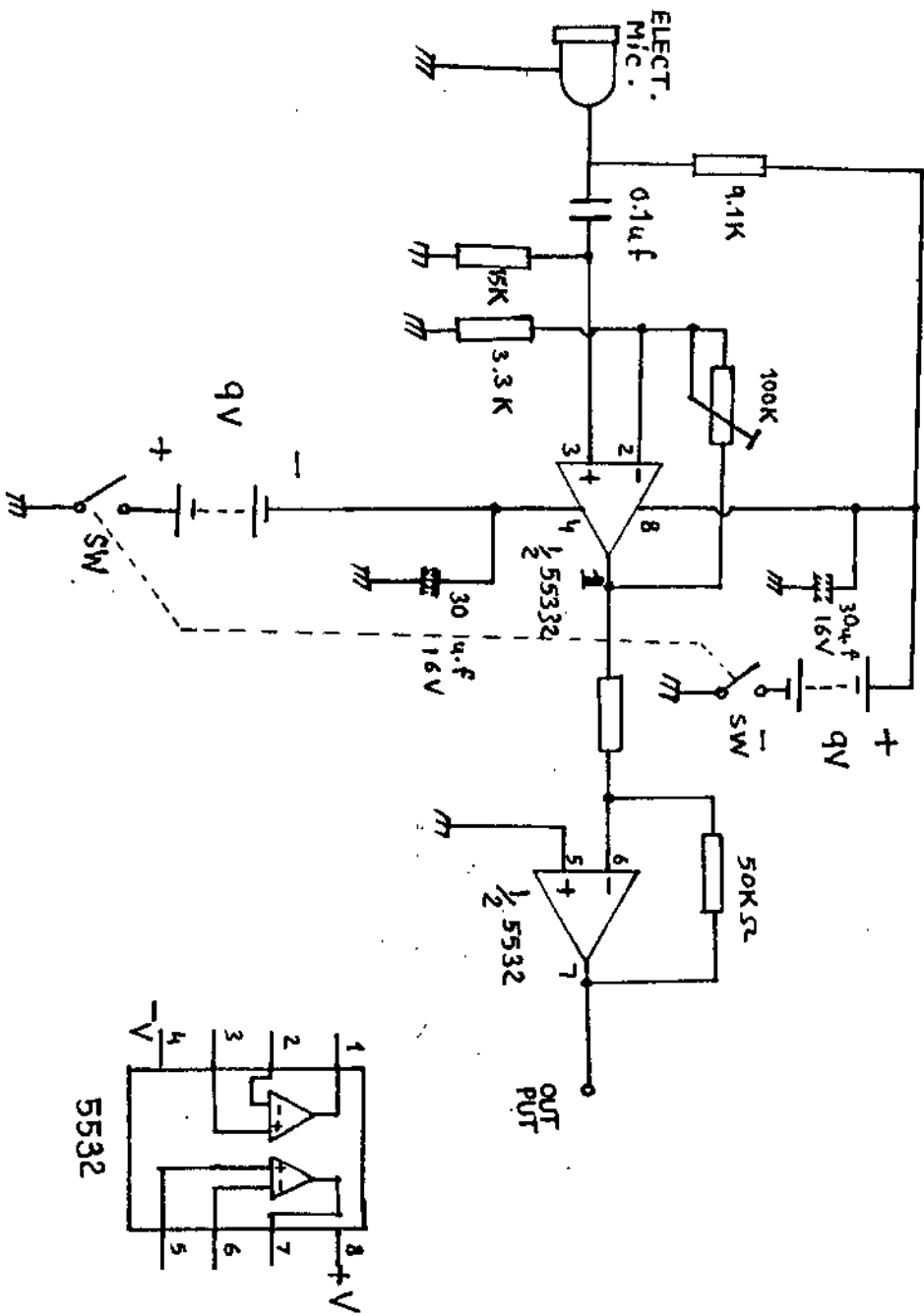
Finally the photoacoustic spectrum of CdS with the wavelength was transformed into the corresponding curve for the variation of the optical absorption coefficient B of CdS with the wavelength λ over the whole tunability range of the dye laser.

Appendices

Appendix A : Low Noisa Preamplifier

Appendix B : Analog Divider.

Low-Noise Preamplifier

ELECT.
Mic.

0.1µf

9.1K

5K

3.3K

100K

3
2
+
−
4
8
½ 5532
1

30µf
16V

30µf
16V

9v
+
−
SW

9v
−
+
SW

50KΩ

5
−
6
+
½ 5532
7

OUT
PUT

5532

1
2
3
4 −V

8 +V
7
6
5

Analog Divider
Model 433J/B

SPECIFICATIONS (typical @ +25°C and ±15V unless otherwise noted)

Model	433J	433B
Transfer Function	$e_o = + \dfrac{10}{9} V_y \left(\dfrac{V_z}{V_x}\right)^m$	*
Rated Output[1]	+10.5V @ 5mA, min	*
Input		
Signal Range	$0 \leq V_x, V_y, V_z \leq +10V$	*
Max Safe Input	$V_x, V_y, V_z \leq \pm 18V$	*
Resistance		
X Terminal	100kΩ ±1%	*
Y Terminal	90kΩ ±10%	*
Z Terminal	100kΩ ±1%	*
External Adjustment of the Exponent, m		
Range for m <1 (Root)	$1/5 \leq m < 1, m = \dfrac{R_2}{R_1 + R_2}$	*
Range for m >1 (Power)	$1 \leq m < 5, m = \dfrac{R_1 + R_2}{R_2}$	*
	$(R_1 + R_2) \leq 200\Omega$	*
Accuracy (Divide Mode)[2,3]		
Total Output Error @ +25°C (for specified input range)		
Typical (RTO)	±5mV ±0.3% of output	±1mV ±0.15% of output
Max Error (RTO)	±50mV	±25mV
Input Range ($V_z \leq V_x$)	0.01V to 10V, V_z	*
	0.1V to 10V, V_x	
Over Specified Temp. Range	±1%	±1% max
Output Offset Voltage (Not Adjustable)		
Initial @ +25°C	±5mV	±2mV max
Offset vs Temp.	±1mV/°C	±1mV/°C max
Noise, 10Hz to 1kHz		
$V_x = +10V$	100μV rms	*
$V_x = +0.1V$	300μV rms	*
Bandwidth, V_y, V_z		
Small Signal (-3dB), 10% of DC Level		
V_y or V_z		*
$V_y = V_z = V_x = 10V$	100kHz	
$V_y = V_z = V_x = 1V$	50kHz	
$V_y = V_z = V_x = 0.1V$	5kHz	
$V_y = V_z = V_x = 0.01V$	400Hz	
Full Output (V_y or $V_z = 5VDC$ ±5VAC)	$(V_x) \times (5kHz)$	
Reference Terminal Voltage[1]		
V_{ref} (Internal Source)	+9.0V ±5% @ 1mA	*
vs Temp (0 to +70°C)	±0.005%/°C	*
Power Supply Range		
Rated Performance	±15VDC @ 10mA	*
Operating	±(12 to 18)VDC	*
Temperature Range		
Rated Performance	0 to +70°C	-25°C to +85°C
Storage	-55°C to +125°C	-55°C to +125°C
Mechanical		
Case Size	1.5" x 1.5" x 0.62"	*
Mating Socket	AC1038	*
Price		
(1–9)	$75	$87
(10–24)	$69	$77

*Same specifications as 433J.
[1] Terminals short circuit protected to ground.
[2] Accuracy is specified in divide mode which is a worst case condition. Input range is 10mV to 10V for specified accuracy when connected as a multiplier.
[3] Error is defined as the difference between the measured output and the theoretical output for any given pair of specified input voltages.
Specifications subject to change without notice.
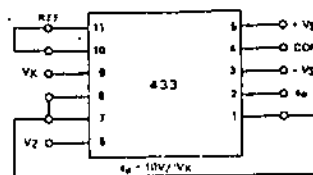
OUTLINE DIMENSIONS
Dimensions shown in inches and (cm).

1.50 (3.81)
0.62 MAX (1.58)
0.20 to 0.25 (0.5 to 0.64)
0.04 DIA (1.02 mm)
1.50 (3.81)
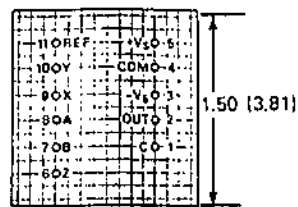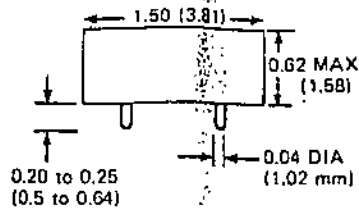
Bottom View
0.10 GRID (0.25)
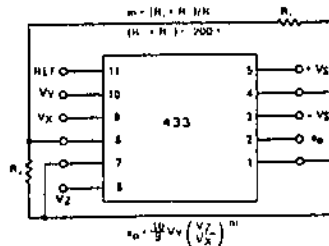
Mating Socket AC 1038
$3.00 (1–9)

WIRING CONNECTIONS
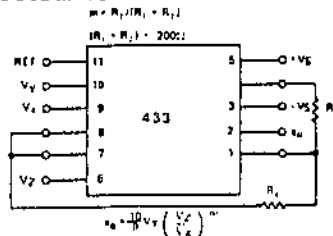Bottom View Shown in All Cases

DIVIDE MODE m = 1

POWERS m >1

ROOTS m <1

REFERENCES

1. Wendlandt, W.W., and Hecht, H.G (1966). Reflectance Spectroscopy, Wiley, New York.

2. Bosquet, P. (1974). Spectroscopy and Its Instrumentation, Crane-Russack New York.

3. Wilks, P.A., Jr., and Hirschfeld, T (1968). Appl. Spectrosc. Rev. 1, 99.

4. Wright, G.B. (Ed.) (1969). Light Scattering of Solids, Springer-Verlag, Berlin and New York.

5. Rosencwaig, A (1978). In Advances in Electronics and Electron Physics, Vol. 46 (L. Marton, Ed.), pp. 207-311, Academic Press, New York.

6. Hey, E., and Gollnick, K (1968). Ber Bunsenges. Phys. Chem. 72, 263.

7. Harshbarger, W.R., and Robin, M.B. (1973) Acc. Chem. Res. 6, 329.

8. Rosencwaig, A. (1973). Opt. Commun. 7, 305

9. Parker, J.G. (1973). Appl. Opt. 12, 2974.

10. Rosencwaig, A., and Gersho, A (1975). Science 190, 556. See also J. Appl. Phys. 47, 64.

11. Bennett, H.S., and Forman, R.A. (1976). Appl. Opt. 15, 2405.

12. Aamodt, L.C., Murphy, J.C., and Parker, J.G. (1977). J. Appl. Phys. 48, 927.

13. Wetsel, G.C., Jr., and McDonald, F.A. (1977), Appl. Phys. Lett. 30, 252.

14. Wetsel, G.C., Jr., and McDonald, F.A. (1977) Bull. Am. Phys. Soc. <u>22</u>, 295.

15. Kinsler, L.E., and Frey A.R. (1962). Fundamentals of Acoustics, Chapter 9, Wiley, New York.

16. Rosencwaig, A. Anal. Chem. 47, 592A, (1975).

17. Rosencwaig, A. Phys. Today 28, (9), 23, (1975).

18. Pankove, J. I. Optical Processes in Semiconductors, Prentice-Hall, New York, (1971).

19. Spectra-Physics, Inc., Handbook Issue A/375 3/14/75.